

Recent Advances in Multi-modal 3D Scene Understanding: A Comprehensive Survey and Evaluation

Yinjie Lei, Zixuan Wang, Feng Chen, Guoqing Wang, Peng Wang and Yang Yang[†]

Abstract—Multi-modal 3D scene understanding has gained considerable attention due to its wide applications in many areas, such as autonomous driving and human-computer interaction. Compared to conventional single-modal 3D understanding, introducing an additional modality not only elevates the richness and precision of scene interpretation but also ensures a more robust and resilient understanding. This becomes especially crucial in varied and challenging environments where solely relying on 3D data might be inadequate. While there has been a surge in the development of multi-modal 3D methods over past three years, especially those integrating multi-camera images (3D+2D) and textual descriptions (3D+language), a comprehensive and in-depth review is notably absent. In this article, we present a systematic survey of recent progress to bridge this gap. We begin by briefly introducing a background that formally defines various 3D multi-modal tasks and summarizes their inherent challenges. After that, we present a novel taxonomy that delivers a thorough categorization of existing methods according to modalities and tasks, exploring their respective strengths and limitations. Furthermore, comparative results of recent approaches on several benchmark datasets, together with insightful analysis, are offered. Finally, we discuss the unresolved issues and provide several potential avenues for future research.

Index Terms—3D Scene Understanding, Multi-modal Learning, LiDAR-camera Fusion, 3D Vision-language Model, Deep Learning

1 INTRODUCTION

GIVEN a 3D point cloud and information from another modality, such as 2D images and natural language, multi-modal 3D scene understanding aims to comprehend the semantic meaning of each object and its surrounding environment [1], [2], [3]. A comprehensive understanding of 3D scenes enables the agent to identify the category and location of the entity and create the new-brand content and style of the scene. In contrast to using only the 3D point cloud, the inclusion of 2D images provides additional color and texture information, while the introduction of natural language enables human-computer interaction. Hence, multi-modal 3D scene understanding has become a vital research area in computer vision, with applications in autonomous driving [4], robot navigation [5], and human-computer interaction [6].

Multi-modal 3D scene understanding can be further divided into: (1) **3D+2D scene understanding**. 3D LiDAR point cloud provides sufficient depth and geometric structure information, which are helpful for obtaining the shape and pose of 3D objects. However, they lack color information and texture details, as well as tend to be sparse and disordered for distant objects [7], [8], [9], [10], [11]. On the contrary, 2D camera images often contain rich color, texture, and context, while suffering from the lack

of geometric information and being susceptible to weather and lighting conditions [12], [13], [14], [15]. Naturally, leveraging the complementarity between LiDAR point cloud and camera images can achieve a better and more complete perception of the 3D environment. However, discrepancies often arise in the representations of the same 3D scene acquired by these two sensors, as LiDAR sensors capture point cloud through a 360-degree rotation whereas cameras capture images from a perspective view without a sense of depth [16]. To solve this problem, some 3D+2D scene understanding approaches are proposed to perform LiDAR-camera fusion via geometry-based alignment [17] and semantic-based alignment [18]. Based on the fused features, these approaches can further perform 3D object detection and segmentation [19], [20], [21], commonly applied in autonomous driving and robot navigation. (2) **3D+language scene understanding**. Traditional 3D scene understanding typically requires users to possess professional expertise, which is not friendly to ordinary users [22], [23], [24], [25], [26], [27]. Users now anticipate a more convenient way to convey their intentions to the computer, achieving information exchange and gaining personalized results. To achieve convenient human-computer interaction, researchers propose the 3D+language scene understanding. It adopts 3D visual information in conjunction with natural language as input [28], [29], [30], since natural language can be served as background knowledge and query conditions to reflect user intentions. By multi-modal interaction, often employing techniques such as the Transformer [31], [32] or graph neural network [33], [34], 3D+language scene understanding approaches can not only locate the entities mentioned by users (e.g., visual grounding and open-vocabulary recognition) but also generate user-required content (e.g., dense captioning, visual question answering, scene generation).

Despite the fact that numerous methods have emerged in recent years, a large part of the multi-modal 3D scene understanding

- Yinjie Lei and Zixuan Wang are with the College of Electronics and Information Engineering, Sichuan University, Chengdu, 610065, China. E-mail: yinjie@scu.edu.cn, zixuan@stu.scu.edu.cn.
- Feng Chen is with the School of Computer Science, University of Adelaide, 5005, Adelaide, Australia. E-mail: chenfeng1271@gmail.com.
- Guoqing Wang, Peng Wang and Yang Yang are with the School of Computer Science and Engineering, University of Electronic Science and Technology of China, Chengdu, 611731, China. E-mail: gqwang0420@hotmail.com, p.wang6@hotmail.com, yang.yang@uestc.edu.cn.
- Corresponding author: Yang Yang (yang.yang@uestc.edu.cn).

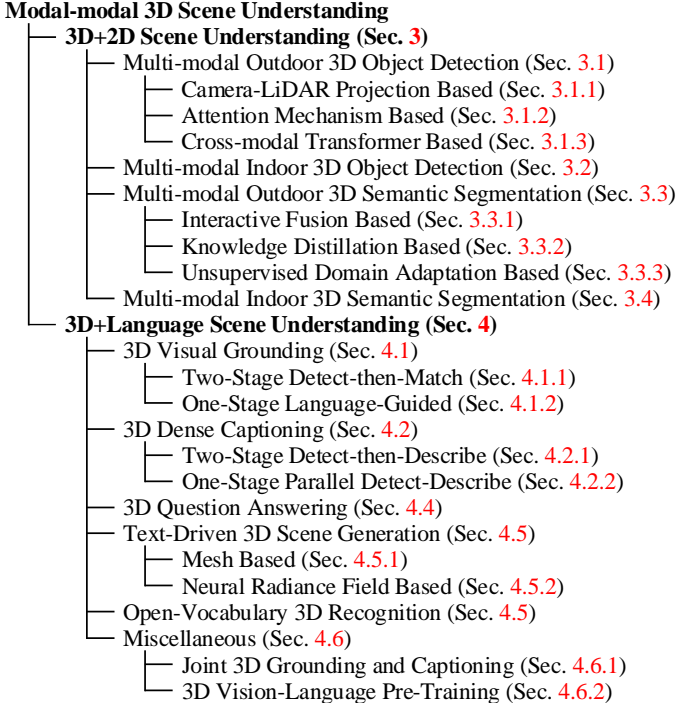


Fig. 1. Taxonomy of representative 3D+2D and 3D+language scene understanding approaches.

remains rather scattered in different tasks, and no such systematic surveys exist. Therefore, it is necessary to systematically summarize recent studies, comprehensively evaluate the performance of different approaches, and prospectively point out future research directions. This motivates this survey that will fill this gap. The major contributions of this paper can be summarized as:

- **Systematic survey of multi-modal 3D scene understanding.** To the best of our knowledge, this is the first survey to thoroughly discuss the recent advances in multi-modal 3D scene understanding. To provide readers with a clear comprehension of our article, we categorize algorithms into different taxonomies from the perspective of both required data modality and target downstream tasks, as shown in Fig. 1.
- **Comprehensive performance evaluation and analysis.** We compare the existing multi-modal 3D scene understanding approaches on several publicly available datasets. Our in-depth analysis can help researchers in selecting the baseline suitable for their specific applications while also offering valuable insights about the modification of existing methods.
- **Insightful discussion of future prospects.** Based on the systematic survey and comprehensive performance comparison, some promising future research directions are discussed, including large-scale 3D foundation model, data-efficient training, computational efficiency of 3D modeling, and incorporation of additional modalities.

The structure of this paper is organized as follows. Sec. 2 summarizes the problem definition and primary challenge in multi-modal 3D scene understanding. Secs. 3 and 4 provide in-depth explorations of typical approaches used for different downstream tasks in 3D+2D and 3D+language scene understanding, respectively. Sec. 5 introduces the benchmark datasets and evaluation

metrics, as well as the comparative analysis of different techniques. Finally, Sec. 6 concludes this paper and discusses the promising avenues for future research.

2 BACKGROUND

2.1 Problem Definition

Multi-modal 3D scene understanding can be divided into two main branches, including 3D+2D scene understanding and 3D+language scene understanding, according to the data modality adopted by the approaches.

The 3D+2D multi-modal scene understanding utilizes the complementary information from the 2D multi-camera image and 3D point cloud to perform 3D object detection and semantic segmentation. Specifically, 3D object detection is intended to localize and recognize objects within a 3D scene, *i.e.*, predicting 3D bounding boxes as well as semantic classes of objects from point clouds [35]. 3D semantic segmentation aims to classify each point in the 3D scene into different semantic categories [36]. In application, some approaches focus on the indoor scene, while others pay attention to the outdoor scene. There are two differences between the indoor and outdoor scene understanding approaches. From the data perspective, the 3D point cloud data for indoor scene understanding approaches is derived from the RGB-D scanner, while that of outdoor scene understanding approaches is derived from the LiDAR sensor. From the application perspective, indoor scene understanding usually aims to help a robot know what is in a scene and where things are. Outdoor scene understanding algorithms are primarily used in autonomous driving, which can perceive the surrounding environment in real-time and determine the type of each object for planning interaction.

The 3D+language multi-modal scene understanding learns the semantic relationships between the 3D point cloud and the given textual description to perform recognition and generation in an interactive manner. Specifically, 3D visual grounding is intended to locate desired objects or regions in the 3D point cloud scene based on the object-related linguistic query [37]. 3D dense captioning aims to identify all possible instances within the 3D point cloud scene and generate the corresponding natural language description for each instance [38]. The goal of 3D visual question answering is to comprehend an entire 3D scene and provide an appropriate answer [39]. Text-guided scene generation is to synthesize a realistic 3D scene composed of complex background and multiple objects from natural language descriptions [40]. Open-vocabulary 3D recognition aims to identify and localize 3D objects of novel classes defined by an unbounded (open) vocabulary at inference, which can generalize beyond the limited number of base classes labeled during the training phase [41].

2.2 Unique Challenges

We summarize the challenges in multimodal 3D scene understanding from (1) cross-sensor calibration, (2) 3D-language alignment, and (3) complex scene understanding.

Cross-sensor Calibration. Cross-sensor calibration endeavors to extract complementary information from cameras and LiDARs, facilitating a cohesive perception of the environment. The challenge, however, lies in effectively fusing 2D images with 3D point cloud. Given the heterogeneous representations between RGB images and point cloud, it is imperative to precisely align features prior to their aggregation. However, due to the inherent sparsity

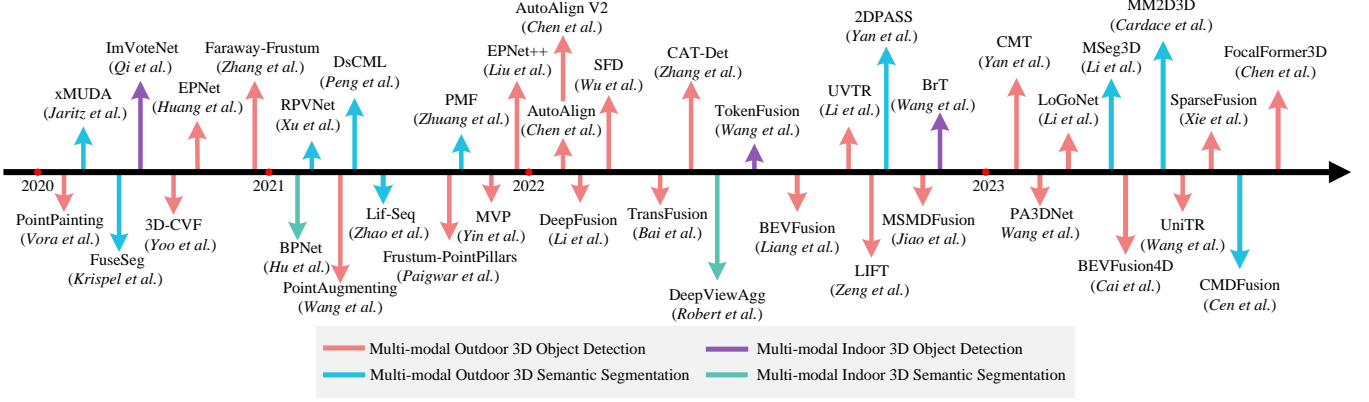


Fig. 2. Chronological overview on 3D+2D multi-modal scene understanding approaches from 2020 to the present, including methods designed for multi-modal outdoor/indoor 3D object detection and multi-modal outdoor/indoor 3D semantic segmentation.

of point cloud, a substantial portion of appearance data from the RGB images is lost when projected onto LiDAR coordinates, complicating the task of assimilating appearance information from the projected RGB images [42].

Another concern pertains to the restricted application potential. The different Field of Views (FOVs) between cameras and LiDARs present a challenge in establishing point-to-pixel mapping for points outside the image planes. Typically, there is only a minimal overlap in the FOVs of LiDARs and cameras. This discrepancy considerably narrows the scope of fusion-based methods [43]. Furthermore, these fusion-based methods tend to be more resource-intensive as they simultaneously process images and point cloud, either through multitask or cascade approaches, during inference. This imposes a significant strain on real-time application demands.

3D-language Alignment. 3D-language alignment seeks to localize the same object from 3D and language modalities. However, it suffers from ambiguous language understanding and intricate 3D geometry representation.

Language typically involve words that describe appearance attributes, object categories, spatial relationships, etc. This requires the model to integrate multiple cues to locate the target object. However, existing research often fails to capture discriminative attributes to exclude the target object from tremendous potential candidates [44]. This shortfall arises from that the sentence-level representation incorporates extraneous data related to ancillary objects. Furthermore, implicit cross-modal attention disproportionately emphasizes the correlation between the 3D object and the object category, often ignoring other critical properties such as appearance and relational dynamics [45].

Moreover, in 3D-language alignment, point cloud processing plays a vital role. The intricate 3D geometries inherent in point cloud can consist of millions of vertices, edges, and faces. This presents challenges when trying to align this high-dimensional data with the comparatively low-dimensional nature of textual descriptions. Existing work [44], [39] mainly treats language as an input condition to correlate point cloud features via attention in grounding, dense caption, and question answering. However, such an implicit interaction may not be the optimal way to bridge the gap between their intrinsic characteristics. Furthermore, textual representations are always unable to align seamlessly with the singular granularity of 3D scenes, given that textual descriptors

can allude to objects at disparate scales, such as referencing both “buildings” and “bricks”.

Complex Scene Understanding. We divide the complex 3D scene into indoor scene with high semantic content and outdoor scene with dynamic and scale.

Indoor scenes are inherently rich in semantic content, showcasing a myriad of object categories, spatial roles, inter-object relationships, and intricate nuances. When discussing object diversity, one observes an array of objects within indoor spaces, ranging from furniture and decorations to appliances and personal items, each imbued with its unique semantic significance. Regarding spatial functionality, each indoor area typically serves a specific function: dining areas cater to eating, whereas studios are designated for work. This specificity is often derived from the objects present and their spatial arrangements. For the relational aspect, objects within these scenes exhibit a logical or functional relationship in their placements. For instance, TVs are conventionally positioned opposite sofas or chairs, and books usually occupy shelves. Lastly, comparing to outdoor scene, indoor scene frequently has a greater depth of detail, evident in the myriad of materials, textures, and colors present. In view of this, capturing such a tremendous context is nontrivial.

The outdoor scene is characterized by its vast scale and temporal dynamic. Firstly, the vast scale and unbounded nature of outdoor scenes, in contrast to indoor settings, make it particularly challenging to capture and process the entirety of the scene. Additionally, the dynamic nature of outdoor environments, where moving vehicles, pedestrians, and other mobile objects frequently appear and disappear, introduces complexities [46], especially when these entities occlude significant elements of the scene.

3 3D+2D MULTI-MODAL SCENE UNDERSTANDING

The 3D+2D multi-modal scene understanding can be subdivided into the multi-modal outdoor/indoor 3D object detection and multi-modal outdoor/indoor 3D semantic segmentation. The chronological overview of existing 3D+2D multi-modal approaches from 2020 to present is shown in Fig. 2.

3.1 Multi-modal Outdoor 3D Object Detection

Recent works of multi-modal outdoor 3D object detection can be divided into three categories: camera-LiDAR projection-based

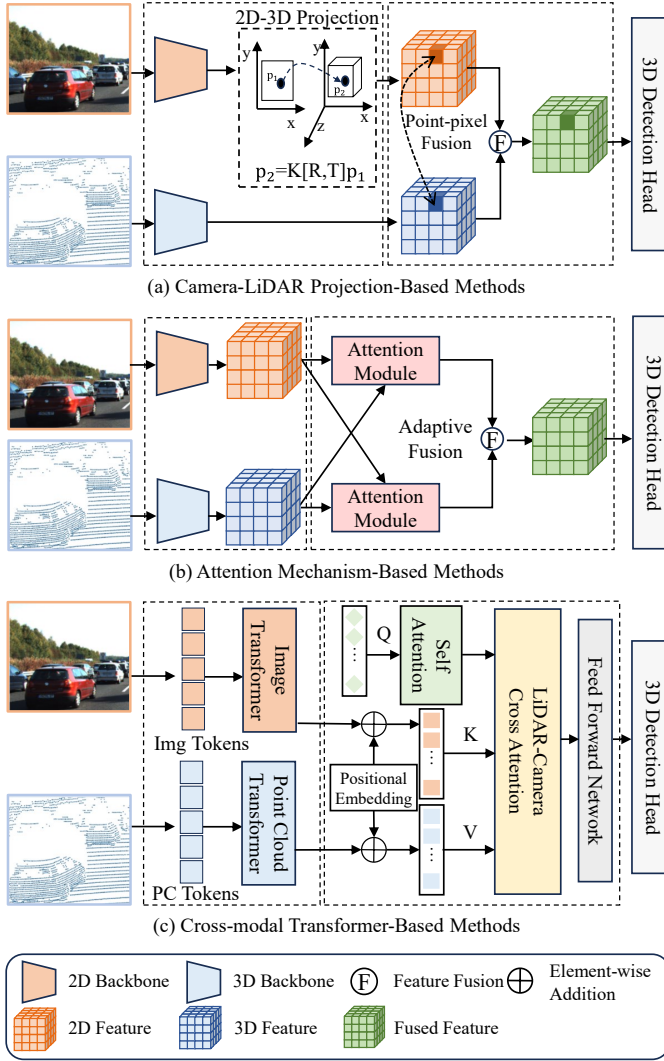


Fig. 3. Overview of multi-modal outdoor 3D object detection pipelines across different categories. From top to bottom: (a) camera-LiDAR projection-based methods, (b) attention mechanism-based methods, and (c) cross-modal Transformer-based methods.

methods, attention mechanism-based methods, and cross-modal Transformer-based methods. General pipelines of them are shown in Fig. 3.

3.1.1 Camera-LiDAR Projection-Based Methods

Camera-LiDAR alignment requires geometric consistency between 3D point cloud and 2D multi-view images because LiDAR sensors and RGB cameras employ different coordinate systems for data representation. To establish geometric consistency between 3D point features and 2D pixel features, camera-LiDAR projection-based methods are proposed. These approaches, as illustrated in Fig. 3 (a), often project 2D image information into the 3D spaces via camera’s intrinsic parameters (*e.g.*, focal length and principal point coordinates) and extrinsic parameters (*e.g.*, camera position and camera orientation). With such consistency, these techniques combine point features and up-projected pixel features in a one-to-one correspondence. In early frameworks, such as PointPainting [47], images are sent to a segmentation module to generate 2D segmentation scores, followed by merging each point’s intensity measurement with its corresponding seman-

tic label after mapping 2D segmentation scores into 3D space. These combined features can be used in any LiDAR-only detection approach to produce 3D bounding boxes. Lately, EPNet [48] and EPNet++ [49] employ novel loss functions to enforce confidence consistency between classification and location, as well as semantic consistency between two modalities. PointAugmenting [50] improves point cloud representation using features derived from the CNN-based 2D detection model. Compared to segmentation maps, such CNN features are more robust to variation in object appearance. MSMD Fusion [51] adopts an approach for point cloud feature enhancement based on virtual points. In particular, all 2D image pixels, along with their semantic information, are first lifted into 3D voxel space via depth completion (these lifted pixels are referred to as “virtual points”). Under the guidance of real voxels, informative virtual points are then adaptively selected and aggregated in groups for sufficient multi-modal interaction. These methods can accurately detect large objects near the LiDAR sensors, however, faraway and small objects are hard to identify because those objects only comprise sparse measurements that even humans cannot clearly see.

To detect faraway objects, several methods rely on the 2D image to recognize the category of each faraway object, because the shape of the object does not change sharply with the increase in depth. Then, 2D instance segmentation masks or bounding boxes are extruded into 3D frustums for locating those objects in 3D space. For instance, Frustum-PointPillars [52] employs the PointPillars [53] to localize smaller objects within the 3D frustum. Faraway-Frustum [54] predicts the centroid of each 3D frustum via point-cloud clustering to determine potential faraway objects. MVP [55] further addresses the density disparities between objects located at varying distances using 3D virtual points. Specifically, dense 3D virtual points near foreground frustum instances are created and combined with original LiDAR points to increase the measurement consistency of the point cloud between close and faraway objects.

3.1.2 Attention Mechanism-Based Methods

Typical camera-LiDAR projection-based approaches often rely on simple techniques like concatenation or element-wise summation/mean operations for merging features from different modalities, treating different features as equally important and neglecting differences of multi-modal or multi-view features. In real-world scenarios, 2D RGB images usually have noisy information caused by occlusion or overcrowded backgrounds. Directly combining noisy 2D images with 3D point cloud without considering the feature importance may impair 3D detection accuracy. Inspired by attention mechanisms in computer vision [56], [57], many researchers have begun to design novel attention mechanism-based frameworks for multi-modal 3D detection. As shown in Fig. 3 (b), this line of research selectively incorporates the features of the current modality with respect to the features from the other modality in an adaptive manner.

Recent advanced approaches combine point cloud features with image features across the whole scene based on the attention mechanism. Some works perform global fusion via channel attention mechanism, which concatenates camera and LiDAR features under the same space along channel dimension and recalibrates the importance of each channel in a learnable manner. For example, BEVFusion [58] employs dual-stream encoders to map camera and LiDAR features into a common BEV space and subsequently performs multi-modal feature fusion based on the Squeeze-and-

Excitation attention mechanism [59]. Similarly, PA3DNet [60] maps camera and LiDAR features into a common voxel space and calculates the importance of different modalities using learnable linear channel attention weights. However, the global channel attention mechanism discards useful spatial information, ignoring differences in pixels and points at different positions. Other approaches, like DeepFusion [61], employ the cross-attention mechanism to overcome such issue. Specifically, in the cross-attention mechanism, LiDAR features are regarded as queries, and camera features are served as keys and values. For each query, the inner product between this query and keys is conducted to generate an attention affinity matrix that represents feature correlations between the current 3D point and all camera pixels. Then, values containing camera information are weighted and aggregated using the attention affinity matrix. Compared to channel attention, the cross-attention mechanism can consider similarities of all pixel-point pairs, enabling each 3D point dynamically attend relevant 2D pixels instead of one-to-one matching. These global fusion approaches, however, may struggle to detect faraway objects which only occupy a small portion of the entire 3D scene. This is because redundant dense representations interfere with the computation of attention weights.

Inspired by MV3D [62] and AVOD [63], several approaches crop foreground instances from a whole scene and then separately apply the attention mechanism in each pair of instances, avoiding negative effects from irrelevant objects and background information. For example, SparseFusion [64] is an efficient framework based on sparse candidates and representations. First, SparseFusion utilizes dual-stream detectors to capture instances from camera and LiDAR modalities. After mapping instance features from each modality into the unified 3D space, SparseFusion fuses them via a lightweight channel attention module in a soft manner. Different from SparseFusion, SFD [65] employs 3D region-of-interest to crop instances from original and virtual point clouds and fuses each pair of instances based on the Squeeze-and-Excitation attention mechanism in a voxel-to-voxel manner. These local fusion approaches, however, suffer from the absence of 2D information during the instance generation stage, causing inaccuracy in instance identification.

To simultaneously consider the global context of each instance (*e.g.*, relations between each instance and a whole scene, as well as relations between each instance and other instances in the distance) and the local context of each instance (*e.g.*, relations between each instance and its surrounding environments) from different modalities in an adaptive manner, many efforts harness the benefits of global fusion and local fusion. Some approaches, like 3D-CVF [66], AutoAlign [67], and AutoAlignV2 [68] follow a “*global-to-local*” pipeline. This pipeline, before cross-modal instance interaction, generates 3D region-of-interests from an informative scene which combines point cloud features and image features. 3D-CVF applies the channel attention mechanism in global fusion and local fusion stages. In AutoAlign and AutoAlignV2 frameworks, after dynamically combining each 3D voxel with its corresponding 2D pixels via the cross-attention mechanism, a similarity loss is adopted between paired regional features in 2D and 3D spaces to enhance semantic consistency between point clouds and images. Other technique, mainly like LoGoNet [69], performs global fusion and local fusion in parallel, leveraging complementarity between scene features and instance features. In the global fusion stage, like previous approaches, image features and point cloud features in a common voxel

space are fused by the deformable cross-attention. For each 3D proposal, geometrically aligned pixel features are sampled from image space and fused through the cross-attention mechanism. Finally, information between globally and locally fused features interact with each other via the self-attention mechanism.

3.1.3 Cross-Modal Transformer-Based Methods

Transformer has emerged as a powerful architecture for processing information from diverse modalities [70], [71], [72] due to its advantage of feature alignment and fusion. Numerous endeavors are dedicated to designing the 3D detection framework based on Transformer. The general pipeline of these methods is illustrated in Fig. 3 (c), which mainly employs the modal-specific Transformer to encode the intra-modal contextual information and utilizes the query-based Transformer to perform inter-modal element-wise interactions. Learnable object queries can align the localization of each object across different modalities and encode the instance-specific information (*e.g.* size and orientation of box) via separately interacting with the image and point cloud features.

The pioneering Transformer-based 3D detection approach, CAT-Det [73], employs the Two-stream Transformer and Cross-Modal Transformer to respectively encode intra-modal and inter-modal long-range contexts, generating powerful representations for each object. TransFusion [74], another early Transformer-based 3D detection approach, adopts a specific Transformer decoder-based detection head. The first Transformer decoder layer initializes bounding boxes from the LiDAR point cloud via a sparse set of object queries. The second Transformer decoder layer combines these object queries with pertinent image features according to the spatial and contextual relationships. CMT [75] aims to further imbue object queries and multi-modal tokens with location awareness. Specifically, CMT utilizes the Coordinates Encoding Module to implicitly inject the 3D position information into multi-modal tokens for generating position-aware features and initialize position-guided queries based on the PETR pipeline [76]. To address the challenge of false negatives in 3D detection, often stemming from occlusion and cluttered backgrounds, FocalFormer3D [77] introduces the multi-stage Hard Instance Probing technique into the Transformer architecture, which maintains positive regions from previous stages to omit the easy candidates and focus on the hard candidates (false negatives) during training.

Transformer-based frameworks described above depend on modality-specific encoders followed by additional query-based fusion, incurring non-negligible computational overheads. Hence, building an efficient Transformer 3D detection model based on the unified multi-modal representation is necessary. UVTR [78] performs 3D detection based on unifying multi-modality representations in the voxel space. First, UVTR maps the image and point cloud into the modal-specific voxel space and formulates the unified voxel representation by adding them together. Then, UVTR samples representative features from the unified voxel space via reference positions and performs instance-level interactions by the object query-based Transformer decoder. UniTR [79] processes different modalities through unified modeling and shared parameters. Specifically, after transforming the 2D image and 3D point cloud into token sequences via modality-specific tokenizers, UniTR performs intra-modal representation by a unified Transformer architecture, whose parameters are shared for different modalities. Then, based on both LiDAR-to-camera and camera-to-LiDAR mapping, UniTR conducts cross-modal representation learning via a modal-agnostic Transformer architecture, simulta-

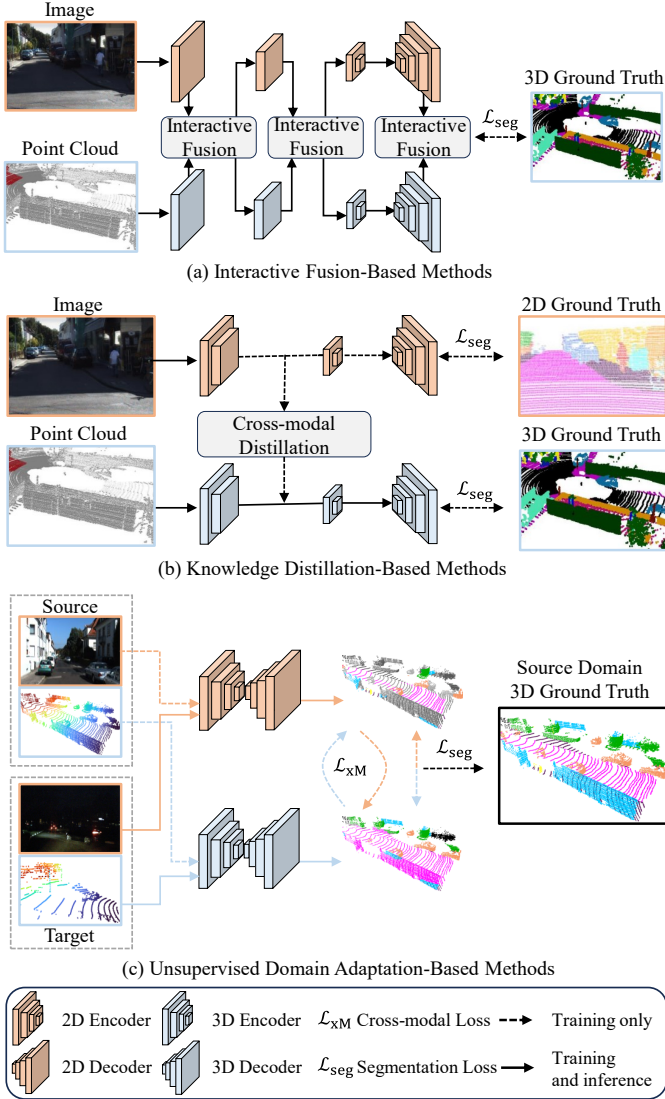


Fig. 4. General pipelines for three categories of multi-modal outdoor semantic segmentation methods. From top to bottom: (a) interactive fusion-based methods, (b) knowledge distillation-based methods, and (c) unsupervised domain adaptation-based methods.

neously considering semantic-aware 2D context and geometry-abundant 3D structural relations.

The complementary views and motion cues encoded in the adjacent frames can improve the accuracy of identifying moving 3D objects. Hence, successful 3D object detection, especially in outdoor autonomous driving scenarios, hinges on the optimal exploitation of all available data across sensors and time. Recent advances in sequential modeling demonstrate that Transformer is very competent in modeling the information interaction for sequential data or cross-modal data. The massive amount of 3D points as a sequence input, however, is computationally prohibitive for Transformer. To model the mutual interaction relationship of cross-sensor data over time in a computationally efficient manner, LIFT [80] is proposed. Specifically, LiDAR frames and camera images are encoded as sparsely-located BEV grid features to reduce the computational overload, as well as a sensor-time 4D self-attention module is designed to effectively and efficiently capture the mutual correlations. Instead of directly aggregating sequential cross-sensor data by a 4D self-attention module, BEVFusion4D

[81] separately performs spatial-domain and temporal-domain feature interaction using different modules. For spatial-domain feature fusion, 2D image features are mapped into BEV features under the guidance of LiDAR spatial prior via the deformable attention module, and then simply concatenated with the LiDAR BEV features. For aggregating spatially-fused BEV features of consecutive frames, the Deformable Transformer-based module dynamically learns the association between temporal features across long spans, aligning temporal features of moving objects without explicit motion calibration.

3.2 Multi-modal Indoor 3D Object Detection

The earliest multi-modal indoor 3D object detection approach, ImVoteNet [42], is centered on the fusing of 2D image votes and 3D point cloud votes. Specifically, ImVoteNet generates 2D votes on image space and lifts them via geometric transformations based on camera parameter. These lifted 2D votes are combined with seed points in the 3D space, serving as the extra semantic and texture information for generating 3D object proposals. After the 2D-3D feature combination, ImVoteNet performs the final object detection based on the VoteNet pipeline [24]. However, simultaneous reliance on both 2D and 3D votes leads to the accumulation of grouping errors.

Transformer architecture proves suitable for addressing grouping errors, owing to its ability to capture long-range dependencies and global contextual information. Despite the effectiveness of Transformer in single-modality 2D [82], [83] and 3D object detection [84], [85], applying it to multi-modal 3D object detection remains challenging because of the modality discrepancy. In order to bridge the geometric and semantic gap between 2D images and 3D point cloud, BrT [86] designs the conditional object query and point-to-patch projection, respectively. Specifically, the conditional object query that unifies the representation of different modalities can be aware of both 2D and 3D coordinates by injecting the aligned position embedding, while the point-to-patch projection fuses the 3D point tokens with its corresponding 2D image tokens to explicitly leverage the semantic relationship between different modalities. TokenFusion [87] effectively combines multiple single-modal Transformers by dynamically detecting useless tokens and substituting these tokens with projected alignment features from the other modality. The novel design of TokenFusion not only enables the Transformer to effectively learn the correlations among multi-modal features but also largely maintains the architecture of the single-modal Transformer unchanged.

3.3 Multi-modal Outdoor 3D Semantic Segmentation

Current approaches of multi-modal 3D semantic segmentation can be roughly divided into three categories, including interactive fusion-based methods, knowledge distillation-based methods, and unsupervised domain adaptation-based methods. General pipelines of these three categories of methods are shown in Fig. 4.

3.3.1 Interactive Fusion-Based Methods

Following U-net architecture, as shown in Fig. 4 (a), interactive fusion-based methods integrate multi-modal features by considering the relationship and complementarity between 2D image and 3D point cloud data, and perform 3D semantic segmentation using the fused features. The pioneering work in interactive fusion-based 3D semantic segmentation is proposed by Meyer et al. [88], which comprises three key components. The first component focuses

on extracting features from 2D camera images and 3D LiDAR measurements, respectively. The second component utilizes the correspondence between LiDAR points and camera pixels to concatenate multi-modal features. The last component feeds the fused features into the pre-trained LaserNet [89] to perform the segmentation. Based on the pioneering framework, FuseSeg [90] further employs MobileNetV2 [91] as a camera branch and utilizes SqueezeSeg [92] as a LiDAR branch to improve the segmentation performance.

Recent studies have further focused on addressing the modality discrepancy between LiDAR and camera data or exploring the complementarity among the range image, point cloud, and voxel. In order to overcome the modal discrepancy, PMF [43] adopts a perception-aware multi-modal feature fusion scheme, in which 2D image features and 3D point cloud features are mutually projected into each other's modalities and simultaneously fused in each modality. On the one hand, 3D point clouds are mapped into the camera coordinate system, generating additional spatial-depth information for 2D RGB images. On the other hand, 2D RGB image features are fused to the 3D LiDAR features, injecting the appearance information into the LiDAR measurement. RPNNet [93] is an adaptive range-point-voxel fusion framework aiming to leverage the density of the range image, the geometric accuracy of the point cloud, and the regularity of the voxel. Specifically, after mapping the range image and voxel data into the feature space of the point cloud, a gated fusion module adaptively merges all three views' representations based on the concurrent inputs.

The above approaches only employ the single-granularity feature fusion strategy. More recently, some hybrid fusion architectures that comprise various feature fusion modules have been designed for multiple and mutual information interactions among different visual modalities. Lif-Seq [94] is a framework based on the coarse-to-fine multi-modal feature fusion, where the coarse fusion aims to leverage the contextual information of the 2D image in a one-to-many manner, and the fine-grained fusion can better align the 2D and 3D features by the offset rectification approach. Specifically, unlike the typical one-to-one manner, in the coarse fusion stage, 3×3 contextual information of each pixel is concatenated to the LiDAR measurement of each 3D point. Then, an offset between the projected image pixel and its corresponding LiDAR point is used to compensate and update the position of the coarse 3D features. The aligned 2D and 3D features are fused for better segmentation. To overcome the limited intersection of the FOV between LiDAR and camera sensors, MSeg3D [95] designs the geometry-based and semantic-based feature fusion. Specifically, the geometry-based feature fusion module completes the missing camera features using predicted pseudo-camera features and fuses LiDAR features with camera features in a one-to-one correspondence via the geometric association. Then, the semantic feature aggregation module aggregates the LiDAR features and camera features into the category-wise semantic embeddings. The embeddings can be regarded as dictionaries that describe the typical characteristics of each category from the perspectives of LiDAR and cameras. Finally, the semantic-based feature fusion module combines geometry-based fused features with semantic embeddings via cross-attention, enabling each point's features to interact with multi-modal semantic embeddings.

3.3.2 Knowledge Distillation-Based Methods

The interactive fusion-based approaches require strictly paired 2D image and 3D point cloud data. However, the FOV of LiDAR

and cameras only overlap in a small portion, leading to an inability to establish a complete and comprehensive point-to-pixel mapping. For instance, only two front-view images are provided by SemanticKITT, while side-view and back-view images are inaccessible [96]. The knowledge distillation-based approaches are proposed to solve such problem. As shown in Fig. 4 (b), these methods distill the 2D prior information into the 3D encoder via multi-view distillation based on a small section of overlap multi-modal data during the training stage. During inference, these methods can perform semantic segmentation without 2D visual input, generalizing to non-overlapped data.

The pioneering approach, 2DPASS [97], employs a fusion-to-single knowledge distillation scheme. Specifically, 2D image features are fused with 3D point cloud features, reserving complete information from multi-modal data. Then, two independent classifiers are separately applied on top of fused and pure 3D features to obtain segmentation scores. Finally, 2DPASS unidirectionally aligns 3D predictions with fusion predictions, transferring the extra 2D information to the 3D encoder as well as maintaining modal-specific information. However, in this scheme, 2D knowledge cannot explicitly be merged into the 3D encoder during training and inference. To address this issue, CMDFusion [98] introduces the bidirectional fusion block with cross-modality distillation. Specifically, CMDFusion adopts a memory branch that stores 2D prior information via cross-modality feature distillation, generating corresponding pseudo-2D features during both training and inference stage. Leveraging this memory branch, the 2D-to-3D directional fusion explicitly enhances the 3D representations by 2D pseudo feature injection, while the 3D-to-2D directional fusion conducts the implicit 3D feature enhancement by pseudo-2D supervision.

3.3.3 Unsupervised Domain Adaptation-Based Methods

Dense labeling 3D point clouds requires massive time consumption. Hence, unsupervised domain adaptation, *i.e.*, applying knowledge learned from source domains with a large number of human annotations to target domains with unlabeled data only, has become a promising research direction in 3D semantic segmentation [99], [100], [101]. Recent studies mainly focus on three real-to-real scenarios, including day-to-night (lighting conditions change), country-to-country (environments change), and dataset-to-dataset (sensor setup change). The general pipeline is illustrated in Fig. 4 (c), which primarily includes cross-domain learning and cross-modal learning. Specifically, cross-domain learning aligns representations across various domains by computing the consistency between source and target predictions within each modality, while cross-modal learning exchanges information across different modalities via KL-divergence minimization between 2D and 3D predictions in each domain.

Building upon the baseline, some approaches are proposed to solve the unique domain shift challenge in the multi-modal 3D scenario, that is, different sensors can be impacted differently by the domain shift, *e.g.*, the camera is influenced by the day-to-night change while LiDAR is robust. A pioneering domain adaptation-based 3D semantic segmentation approach, xMUDA [102], [103], leverages the complementarity of cross-modal learning and self-training. Cross-modal learning can teach the different modalities to be aware of each other via mutually estimating the prediction, enabling modality susceptible to domain shift to become more robust. Once cross-modal learning is finished, for the target domain, high-confidence labels based on the predicted probabilities

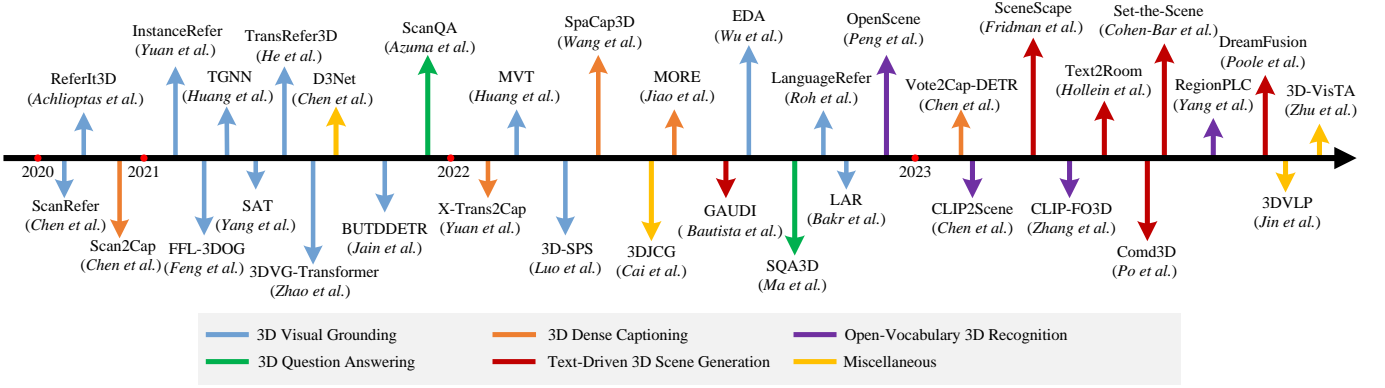


Fig. 5. Chronological overview on 3D+language multi-modal scene understanding approaches from 2020 to the present, including methods designed for 3D visual grounding, 3D dense captioning, joint 3D visual grounding and dense captioning, 3D question answering, text-driven 3D scene generation, and vision-language pre-training.

are selected as pseudo-labels offline. Then, self-training can be performed based on generated pseudo-labels, which effectively leverage unlabeled data to help model learning both characteristics and distributions of the target domain. Lately, MM2D3D [104] introduces the perception-aware multi-sensor fusion module (mentioned in PMF [43]) into the unsupervised domain adaptation framework, enabling the model more robust to the domain shift. The effectiveness of this module is because depth information injected into the 2D encoder is less influenced by the domain gap (e.g., lighting conditions change), and RGB information fused into the 3D encoder provides more semantic features (e.g., dark pixels in images acquired at night).

However, the above methods align multi-modal features in a one-to-one correspondence, which can only achieve information interaction between matched 3D and 2D features, discarding useful information in those unmatched ones. DsCML [105] designs a dynamic sparse-to-dense cross-modal learning to address this issue, where features of an individual 3D point can interact with those of dense relevant 2D pixels. This effective design is inspired by the fact that neighboring pixels likely belong to the same category, as well as all the same-categorized pixel features should be sampled to exchange information with the corresponding 3D point feature. Specifically, for each 3D point, DsCML utilizes the deformable convolution [106] to adaptively search the patch of the 2D feature map with appropriate size, dynamically capturing related 2D pixel features with the same category. Once the classifier has handled features, a sparse-to-dense loss is used to align the supremum and infimum of a set of 2D probability scores with their corresponding individual 3D probability score, exchanging the information between different modalities in a many-to-one manner.

3.4 Multi-modal Indoor 3D Semantic Segmentation

Early multi-modal indoor 3D semantic segmentation approaches, like 3DMV [107], 3D-SIS [108], and MVPNet [109], usually combine projected 3D features from 2D images with 3D point cloud features to assist 3D segmentation. Although direct and feasible, there are still two challenges. On the one hand, they process 2D images and 3D point clouds individually, so they cannot fully utilize the complementary information inside 2D and 3D data. On the other hand, a 3D point is usually seen in different 2D images, while current approaches can hardly merge multi-view

images meaningfully. To facilitate information inside the 2D and 3D modalities flow bidirectionally at the network architectural level, BPNet [110] employs a bidirectional projection module to fuse the multi-view 2D and 3D features in both directions. Specifically, the projection link matrix between 2D and 3D encoders is built at each level, and the features are transferred bidirectionally according to this link matrix, *i.e.*, 2D features are mapped into the 3D space to enhance the 3D representations and vice versa. In an effort to effectively aggregate features between multiple views, DeepViewAgg [111] introduces a learnable attention-based multi-view aggregation scheme that utilizes the viewing conditions of 3D point cloud to merge the most relevant features from 2D images taken at arbitrary positions.

4 3D+LANGUAGE MULTI-MODAL SCENE UNDERSTANDING

The 3D+language multi-modal scene understanding can be divided into 3D visual grounding, 3D dense captioning, 3D question answering, text-driven 3D scene generation, open-vocabulary 3D recognition, and miscellaneous. The chronological overview of existing 3D+language multi-modal approaches from 2020 to the present is shown in Fig. 5.

4.1 3D Visual Grounding

Recent works of 3D visual grounding (VG) can be roughly divided into two categories, including the two-stage detect-then-match and one-stage language-guided schemes.

4.1.1 Two-Stage Detect-then-Match Methods

Inspired by the approaches in 2D counterparts [113], [114], [115], most 3D VG methods adopt a two-stage scheme that first produces numerous proposals by a pre-trained 3D detector [116], [117], [84] or segmenter [118], [119], [120] (detection stage) and then fuses the feature of the proposal and the feature of linguistic query to discriminate the target object (matching stage). Previous studies mainly focus on the second stage, *i.e.*, exploring relations among proposals to select the best-matched object. For example, ScanRefer [37] directly concatenates features of the proposal and linguistic query, which barely performs satisfactorily because the two modal features are not sufficiently matched. ReferIt3D [121] and TGNN [122] not only concatenate the proposal features and

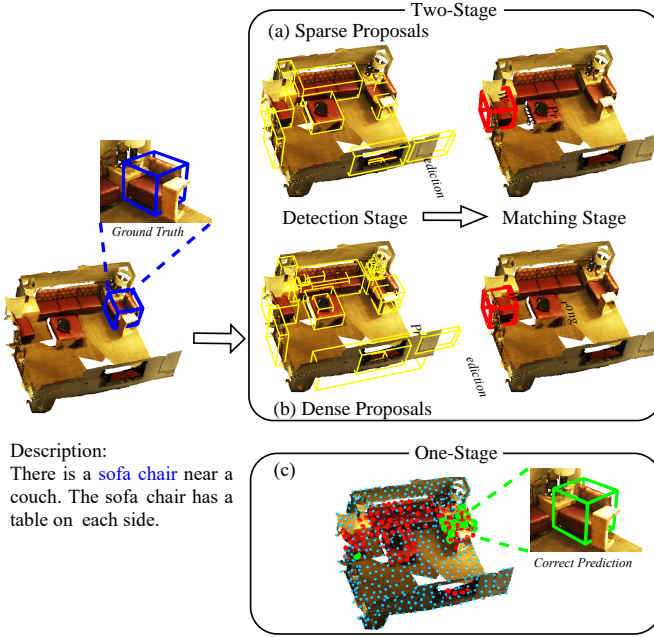


Fig. 6. The diagram of two-stage detect-then-match (upper) and one-stage language-guided (bottom) 3D visual grounding methods [112]. (a) Sparse proposals may overlook the target in the detection stage. (b) Dense proposals may confuse the matching stage. (c) The one-stage method can progressively select keypoints with the guidance of the language description.

the textual embeddings but also encode the relationship among objects by the graph neural network. Further, FFL-3DOG [123] firstly leverages the language scene graph to learn the long-distance phrase correlations, secondly employs the multi-level 3D proposal relation graph to capture the object-object and object-scene co-occurrence relationships, and lastly uses the free-form description guided 3D visual graph to match the global contexts of phrases and proposals. InstanceRefer [124] first performs the instance multi-level contextual referring to explicitly capture instance attributes, instance-to-instance relationships, and instance-to-background global location, and then selects the most relevant instances by the cooperative holistic visual-language feature matching.

Recently, research endeavors have prominently focused on harnessing the Transformer architecture for the purposes of visual-language feature extraction and fusion. For example, LanguageRefer [125], a BERT [126] architecture-based 3D VG method, regards 3D VG as a language modeling problem, which replaces each proposal with its corresponding label of semantic category and predicts the grounding results by a matching process between the language description and each semantic label. 3DVG-Transformer [127] is a relation-aware 3D VG method, which utilizes the coordinate-guided contextual aggregation module for relation-enhanced proposal generation and employs the multiplex attention module to perform cross-modal proposal disambiguation. In order to perform fine-grained 3D VG, TransRefer3D [128] designs the entity-and-relation aware Transformer to model the entities and their relationships among multi-modal contexts. Specifically, Entity-aware Attention is employed to perform matching between the object features and the corresponding linguistic entity features (e.g., category, color, and size), and Relation-aware Attention is utilized to extract visual relation features of object-

object pairs and match them with the linguistic relation features (e.g., comparative relation and spatial relation). The above three approaches study the 3D VG under specific views, however, the visual-language correspondence learned in this way may fail once the view changes. To solve such issue, MVT [129] designs a multi-view Transformer architecture that aims to learn the view-robust multi-modal representation. Specifically, given the 3D scene under the specific view, MVT first projects it to a multi-view space by the equal angle rotation. After fusing the proposal and language features for each view by the Transformer decoder, MVT aggregates information from different views to identify the target object, reducing the dependency on the starting view.

To further overcome the sparse, noisy, and incomplete natures of point cloud, many works attempt to leverage rich and clean 2D visual features to assist 3D VG. For example, SAT [130] utilizes the 2D image semantics, *i.e.*, object label, image feature, and 2D geometric feature, as the extra input in the training stage to facilitate the joint representation learning between the point cloud and language. Specifically, in addition to the traditional VG loss that maximizes the score between the paired positive proposal and language description, SAT also leverages the auxiliary object correspondence losses, learning the correspondence between the proposals in the 3D scene and the ones in the 2D image, to distill the rich and clean semantics of 2D object representation. Instead of using real 2D images, LAR [131] aims to enhance the quality of the 3D visual representation by incorporating corresponding 2D object representation from synthetic images. Specifically, LAR first projects the 3D point cloud into multi-view 2D images through the 2D synthetic images generator. Then, LAR utilizes the multi-modal Transformer-based architecture to capture and fuse the features of the 3D point cloud, 2D synthetic image, and the linguistic query.

However, these two-stage methods face the dilemma of deciding the proposal numbers since the 3D detector adopted in the first stage requires sampling a few keypoints to represent the whole 3D scene and generates the corresponding proposal for each keypoint. As shown in Fig. 6 (a), the sparse proposals may overlook the target in the first stage, thus the target can not be matched in the second stage. As shown in Fig. 6 (b), dense proposals may contain unavoidable redundant objects, leading to the inability to distinguish the target in the second stage because the inter-proposal relationships are too complex. Furthermore, the keypoint sampling strategy is language-irrelevant, which adds difficulty to the detector for identifying the language-concerned proposal.

4.1.2 One-Stage Language-Guided Methods

In contrast to the two-stage 3D VG methods, the object detection and feature extraction in the one-stage 3D VG approach are modulated by the linguistic query, which makes it easier to locate the query-relevant object, as shown in Fig. 6 (c). 3D-SPS [112] progressively selects keypoints with the guidance of the language description. Specifically, 3D-SPS first leverages the description-aware keypoint selecting module to coarsely figure out the language-concerned points and then uses the target-oriented progressive mining module to finely focus on the target object. BUTD-DETR [133] is inspired by MDETR [134] and GLIP [135], which is a bottom-up top-down detection transformer for one-stage 3D VG. Specifically, BUTD-DETR leverages the proposal information (bottom-up) and the language description (top-down) as guidance to decode the target object through a detection head.

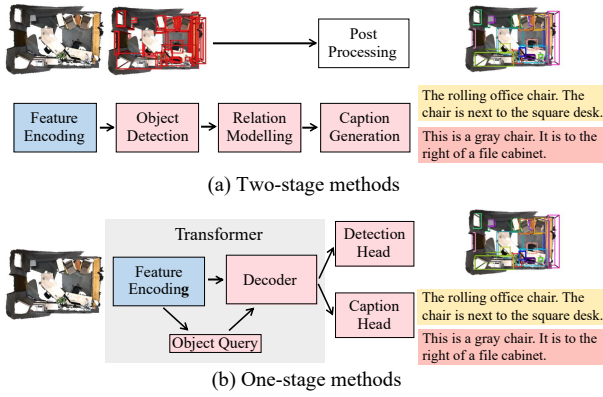


Fig. 7. The diagram of two-stage detect-then-describe and one-stage parallel detect-describe 3D dense captioning methods [132]. (a) The two-stage method relies on the output of the detector. (b) The one-stage method directly feeds the decoder output into the detection and caption heads in parallel.

However, existing one-stage methods either extract the global sentence-level feature coupling all words, which neglect the word-level features. To solve these problems, EDA [136] explicitly decouples the textual attributes in a sentence and performs the dense alignment between the 3D point cloud and the fine-grained linguistic description. First, the input text is parsed to decouple the different semantic components, including the main object word, relations, attributes, and other auxiliary objects. Then, the dense alignment is performed between the candidate 3D objects and multiple related semantic components, achieving fine-grained feature matching. Finally, the candidate object with the highest similarity to the decoupled semantic components rather than the entire sentence is selected as the final grounding object, avoiding the ambiguity resulting from those irrelevant components.

4.2 3D Dense Captioning

Unlike 2D image captioning, which primarily generates an overall description of a given image [137], [138], [139], 3D dense captioning requires a more nuanced understanding of the location and attribute of objects. This difference has led researchers to develop a set of tailored paradigms for 3D dense captioning rather than simply employing existing 2D captioning methods. Broadly, current methods can be grouped into two categories: two-stage detect-then-describe and one-stage parallel detect-describe approaches. Diagrams of them are shown in Fig. 7.

4.2.1 Two-Stage Detect-then-Describe Methods

Two-stage methods usually follow the “detect-then-describe” pipeline, which employs the detection backbone to generate a series of proposals and then create captions for each detected object, as shown in Fig. 7 (a). Current studies mainly focus on modeling the attributes of each object as well as the relationship between several adjacent objects. The pioneering approach Scan2Cap [38] regards each proposal as the node in the relational graph to model the relationship between different proposals, generating an enhanced representation of each proposal. Then, Scan2Cap adopts relational and enhanced features to produce more distinctive descriptions through a context-aware attention captioning module.

However, Scan2Cap has limitations in extracting complex inter-object relations. To capture complex relations in 3D scene, MORE [140] progressively encodes object relations because complex relations can be deduced from a limited of basic ones. Specifically, MORE encodes multiple first-order relations (e.g., on the left) as edges of a graph constructed over 3D proposals. Then, MORE extracts several triplets that encapsulate first-order relations as the basic unit from the previous graph to construct the object-centric triplet graph, inferring multi-order relations (e.g., surrounded by) for every target object. Similarly, SpaCap3D [141] proposes a relative spatiality modeling scheme, where the relation learning among proposals is explicitly supervised to guide the spatial relations encoding.

Another significant development is to transfer the rich texture and color information in 2D images to produce faithful descriptions. Earlier methods [38], [140], [141] employ auxiliary feature extractors to integrate 2D features into the 3D point cloud. While effective, these approaches increase the computational load during the inference stage. To tackle this issue, X-Trans2CaP [142] employs a cross-modal knowledge distillation strategy based on the teacher-student architecture, where the teacher network leverages multi-modal inputs and the student only takes 3D inputs. Specifically, during the training phase, the teacher network employs the feature consistency constraints to guide the student one to learn 2D prior knowledge. Owing to the feature alignment in the training phase, only point cloud need to be fed into the student network during the inference stage to obtain reliable descriptions that implicitly combine information from two modalities.

4.2.2 One-Stage Parallel Detect-Describe Methods

Despite the advancements of two-stage 3D dense captioning methods, some problems persist, including the reliance on the detection backbone performance and inadequate consideration of the reciprocal enhancement between detection and captioning. Inspired by fully Transformer encoder-decoder architecture 3DETR [143], the one-stage 3D dense captioning approach is proposed to solve these issues, which regards 3D dense captioning as the set-to-set problem where each instance and its language description is matched with a query in a one-to-one correspondence manner. As shown in Fig. 7 (b), current one-stage methods follow the “detect-describe parallel” pipeline, which receives a 3D point cloud as the input and generates a set of bounding boxes and linguistic descriptions. Specifically, after generating scene tokens from the 3D point cloud by the feature encoder, learnable object queries are produced from these tokens to represent proposal centers and their semantic information implicitly. Then, the Transformer decoder decodes each object query by parallel heads for detection and captioning. On the basis of the pipeline, Vote2Cap-DETR [132], a pioneering one-stage 3D dense captioning framework, further proposes the vote query and the dual-clued captioner. Particularly, inspired by the VoteNet, the spatial bias of each proposal is encoded via the offset estimation and injected into the original object query for better localization of objects in the cluttered 3D scene. The dual-clued captioner employs the last decoder layer’s output feature of a vote query as the caption prefix to identify the described object, as well as utilizes contextual features surrounding the absolute location of each vote query to provide more information for generating a descriptive caption.

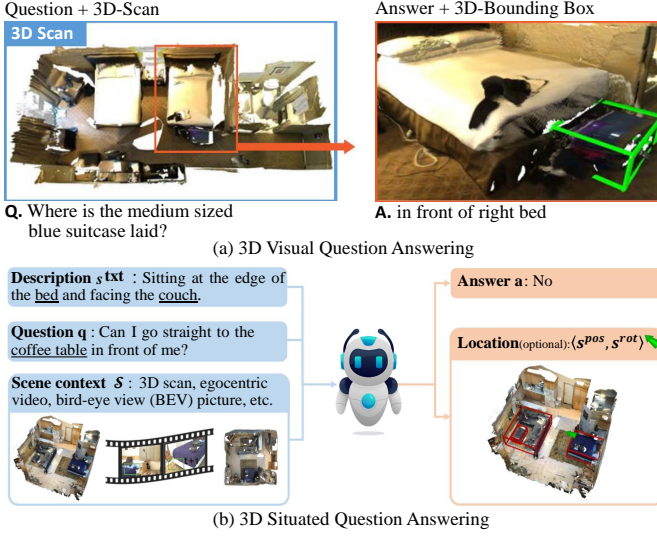


Fig. 8. An illustration of 3D question answering. (a) is 3D visual question answering [39] which requires predicting an answer phrase and the corresponding 3D bounding boxes according to an entire 3D scan and a linguistic question. (b) is 3D situated question answering [144] where agents should comprehend and localize the situation of objects in the 3D scene with a given textual description.

4.3 3D Question Answering

Current studies of 3D question answering can be categorized into 3D visual question answering (VQA) and 3D situated question answering (SQA). The illustrations of 3D VQA and SQA are shown in Fig. 8.

3D VQA focuses on rich and complex scene question answering, which requires the model to have strong spatial perception and reasoning capabilities. ScanQA [39] is the well-known approach designed for 3D VQA, which answers a given question and predicts bounding boxes for described objects in the textual question, facilitating spatial understanding of object direction and location by auxiliary detection loss. Specifically, after obtaining the object proposal representation and word representation via visual encoder and language encoder, ScanQA applies encoder and decoder layers of Transformer to fuse multiple 3D object features guided by language information. Then, ScanQA leverages the fused representations to estimate the bounding box and label of the object, as well as predict the answer associated with the given question and 3D scene.

In addition to the 3D scene and corresponding question, 3D SQA also provides the situation description that elucidates the position and orientation of the agent. The 3D SQA is required to understand the given situation from the first-person viewpoint and answer the question under that situation. SQA3D [144] introduces two baselines, including the 3D model and the zero-shot model. The 3D model is the modified version of the ScanQA model [39], which can further predict the position and orientation of the agent through the location head. The zero-shot model intends to exploit the capabilities of large language models like GPT-3 [145] and Unified QA [146]. Specifically, the zero-shot model employs the off-the-shelf 3D captioning technique to convert the 3D point cloud into captions and feeds these captions along with the situation description into the large language model as prompts to generate a reasonable answer.

4.4 Text-Driven 3D Scene Generation

Text-driven 3D scene generation mainly focuses on synthesizing a realistic 3D scene composed of complex background and multiple objects from natural language descriptions. However, collecting large amounts of scene-description pairs to train a 3D scene generation model from scratch is impractical [147], [148]. Therefore, existing methods mainly circumvent these limitations by using a pretrained 2D text-to-image diffusion model to perform text-driven 3D scene synthesis [149], [150], [151]. These methods can be categorized into (1) mesh-based methods and (2) Neural Radiance Field (NeRF)-based methods, depending on their intrinsic 3D representation manner.

4.4.1 Mesh-Based Methods

Early works, like SceneScape [152] and Text2Room [153], generate the 3D scene by updating the mesh representation [154] in an online fashion. Specifically, SceneScape and Text2Room leverage both content prior and geometry prior information to generate the initial 3D mesh and iteratively render the 3D mesh from the new camera view. The content information and geometry information of each viewpoint are provided by the pre-trained diffusion model and the monocular depth estimation model, respectively. However, SceneScape and Text2Room mainly focus on indoor scene generation and can hardly be applied to outdoor scene generation because of the geometry complexity of the outdoor scene and the shortcomings of the mesh representation.

4.4.2 Neural Radiance Field-Based Methods

Compared to the mesh representation, NeRF [155] can not only model fine-grained information in various scenes but also avoid artifacts caused by a triangular mesh. Dreamfusion [156] introduces a loss based on probability density distillation that enables the use of a 2D diffusion model as a prior for optimization of a parametric image generator. Specifically, Score Distillation Sampling is proposed to optimize a randomly-initialized NeRF via gradient descent such that its 2D renderings from random angles achieve a low loss. GAUDI [157] is a two-stage framework for immersive 3D scene generation, which first employs reconstruction loss to optimize the latent representation of disentangling the camera pose (camera path) and 3D scene (radiance field) and then learns the conditional generative model over the latent representation in the reverse process of DDPM [158]. Comd3D [159] is a compositional 3D scene generation framework based on the locally conditioned diffusion model. Given the 3D scene represented by VoxNeRF and the set of bounding boxes with corresponding natural language descriptions, Comd3D separately applies different diffusion models to specified regions of the VoxNeRF according to the bounding boxes. By defining the bounding box and linguistic prompt, Comd3D allows the user to explicitly control the size and position of the scene component.

However, the above approaches can hardly enable the user to edit the texture and geometry of each component or utilize the component in other scenes because the 3D scene is represented as a whole and different components are interdependent. In view of this, Set-the-Scene [160] employs a set of independent NeRFs as the object proxies to represent a 3D scene and utilizes the local-global training to jointly optimize the representations of both object and scene. Specifically, Set-the-Scene alternates between locally optimizing each object on its own and optimizing the entire scene rendered together as a whole. When optimizing single

object, the corresponding NeRF is rendered on its own from a random viewpoint to learn a complete representation of the object. When optimizing the scene, the rigid transformation is employed to shift the rays to match the desired placement defined by each object proxy, creating a harmonious scene with style match.

4.5 Open-Vocabulary 3D Recognition

Human annotations used in current 3D recognition benchmarks only contain close-set semantic information of objects (*e.g.*, 20 classes in ScanNet [8]). This makes previous supervised learning-based frameworks difficult to recognize open-vocabulary categories and reason open-world semantics. Vision-language foundation models (*e.g.*, CLIP [149]), which possess rich visual and language knowledge via unsupervised learning on image-text pairs from internet, have shown superior ability in open-vocabulary reasoning for classification and dense prediction. Transferring capabilities from CLIP-based models, hence, can benefit open-vocabulary 3D recognition.

To leverage prior knowledge from CLIP-based models, open-vocabulary 3D recognition approaches use 2D images as a bridge to align the embedding space of text and 3D point cloud data. Due to the well-aligned image and text features achieved by CLIP, point cloud features can implicitly align with the text embedding. For example, OpenScene [161] establishes the correspondence between 2D images and 3D point clouds based on the available RGB-D data and employs contrastive learning to align the 2D and 3D representations. Instead of scene-level alignment between 2D and 3D features, CLIP-FO3D [162] focuses on region-level knowledge distillation. Specifically, CLIP-FO3D first adds several local classification tokens to the visual encoder of CLIP, aggregating features from local patches within a region. After projecting local image features to the 3D space, CLIP-FO3D then trains the 3D network by minimizing the distance between learned point features and projected image features. CLIP2Scene [163] aims to train a 3D network via semantic regularization using CLIP knowledge. Specifically, CLIP2Scene first generates dense pixel-text pairs by following the off-the-shelf MaskCLIP framework [164]. Once calibrating the point cloud with corresponding images captured by multi-view cameras, CLIP2Scene produces numerous point-text pairs according to pixel-text pairs. Finally, CLIP2Scene utilizes text semantics to select the positive and negative point samples and employs contrastive learning to train the 3D network. RegionPLC [165] achieves fine-grained 3D scene understanding based on a regional point-language contrastive learning framework. Specifically, after creating dense regional visual prompts and captions based on 2D foundation models, they can be aligned with 3D regions by geometry correspondence to establish fine-grained associations between points and language. With point-language pairs, point-discriminative contrastive learning is then employed to optimal point-wise embedding, which avoids interference from nearby unrelated points as in CLIP-style contrastive loss based on global features.

4.6 Miscellaneous

Some approaches focus on more than one 3D+language multi-modal task, which can be difficult to categorize into any previously mentioned sections. In this section, we elucidate these miscellaneous methods.

4.6.1 Joint 3D Grounding and Captioning

Several studies have demonstrated that 3D VG and dense captioning are naturally complementary. Specifically, 3D VG is relation-oriented, which requires learning relationships among objects for discriminating different objects, especially objects from the same class. On the contrary, 3D dense captioning is object-oriented, which focuses more on learning attributes of the target objects and relationships between the target and its surrounding objects. If 3D VG and dense captioning are integrated into a unified architecture, grounding can provide more relation information to improve captioning performance. Meanwhile, captioning can help enhance grounding performance by providing fine-grained attribute information.

Recently, drawing inspiration from module similarity in two-stage frameworks, some studies have developed unified architectures for joint 3D VG and dense captioning, which leverage the complementary nature between them to improve performance. For example, D3Net [45] unifies 3D VG and dense captioning based on an end-to-end speaker-listener architecture in a self-critical manner. Specifically, the speaker module regards proposals from the point cloud as input to generate dense captions, and the listener matches such captions with proposals to discriminate the target object. In this way, the speaker is able to generate unique captions of each object, which makes it discriminative from similar ones, and the listener can obtain more training data from the speaker to enhance the robustness of grounding. However, D3Net fails to leverage the shared representation of visual or language modality. To address this problem, 3DJCG [166] introduces a shared-specific framework, which is composed of shared task-agonistic modules and lightweight task-specific modules. First, shared task-agonistic modules learn fine-grained attribute features of each object and complex relations between different objects, which benefit both captioning and VG. Then, lightweight task-specific heads solve dense captioning and VG, respectively, by casting each task as a proxy of another one.

4.6.2 3D Vision-Language Pre-Training

Current approaches for 3D vision-language understanding are often task-specific, lacking a foundation model in learning generic cross-modality representation which can be applied in various application scenarios. Consequently, developing a general-purpose 3D visual-language framework is necessary. 3D-VisTA [32] introduces a pre-trained Transformer for 3D scene-text alignment, which can be easily adapted into downstream tasks, ranging from visual grounding and dense captioning to question answering. 3D-VisTA simply utilizes self-attention layers for both single-modal modeling and multi-modal fusion without any sophisticated task-specific design. To further enhance its performance on 3D vision-language tasks, they construct ScanScribe, the first large-scale 3D scene-text pairs dataset for 3D vision-language pre-training. Taking masked language/object modeling and scene-text matching as proxy tasks, such pretraining procedure effectively learns the alignment between 3D point clouds and texts. Concurrently, 3D-VLP [167] proposes to solve limited training data, relational ambiguities, and irregular point cloud structure with context-aware spatial-semantic alignment and mutual 3D-language masked modeling. In detail, context-aware spatial-semantic alignment not only aligns each 3D object to its class noun (semantic-aware) but also aligns it with the corresponding referring expression (context-aware) which conveys complex spatial relations. Mutual 3D-language masked modeling exchanges cross-modality information

by predicting the semantic class of masked 3D objects and the corresponding masked words.

5 PERFORMANCE EVALUATION

This section introduces the benchmark datasets, evaluation metrics, and comparative results of existing methods on different tasks. Considering the vast and complex datasets available, we only introduce the mainstream benchmark datasets that we will be using for various tasks. Additionally, we omit the comparative results of indoor 3D detection, text-driven scene generation and 3D-language pre-training, due to insufficient entries submitted to official datasets, and inconsistent experimental settings&metrics.

5.1 Datasets

KITTI [11] is one of the most popular benchmark datasets for 3D object detection and orientation estimation in autonomous driving, which comprises more than 200,000 annotated point cloud scenarios consisting of cars and pedestrians. This dataset includes not only point cloud but also stereo and optical flow data, which is collected using several pieces of equipment, including four video cameras, a laser scanner, and a localization system. Specifically, 7,481 samples with annotations in the camera field of vision are used for training and the other 7,518 samples are remained for testing. According to the occlusion level, visibility, and bounding box size, the samples are further divided into three difficulty levels, including easy, moderate, and hard.

nuScenes [168] is another multi-modal autonomous driving dataset provided by the full sensor suite, including cameras, radars, and LiDARs. Specifically, the nuScenes dataset contains 1,000 scenes. Each scene has approximately 40,000 frames, where 28,130/6,019/6,008 frames are regarded as training/validation/testing samples. For 3D object detection, after merging similar classes and removing rare classes, the key samples are annotated with ground truth labels of 10 foreground object classes at a frequency of 2Hz. For 3D semantic segmentation, every point in the keyframe is annotated using 6 more background classes in addition to the 10 foreground object classes.

SemanticKITTI [96] is a large-scale outdoor-scene dataset for 3D semantic segmentation, which annotates all data of KITTI Vision Odometry Benchmark [11] and provides dense point-wise annotations for the complete 360 field-of-view of the employed automotive LiDAR. For consistency with the KITTI Vision Odometry Benchmark, the SemanticKITTI dataset employs the same division for our training and test set. It is worth noting that SemanticKITTI provides as many as 28 classes, but the official evaluation only uses a set of 19 valid classes due to ignoring classes with only a few points and merging classes with different mobility states.

ScanRefer [37] is a large-scale dataset for 3D visual grounding and dense captioning. The dataset contains 51,583 human-written free-form descriptions of 11,046 objects based on the 800 ScanNet scenes [8]. The object descriptions cover more than 250 common indoor objects, such as sofas, chairs, table lamps, etc., and include information about the object’s appearance and spatial relationship with other objects. ScanRefer dataset follows the ScanNet benchmark to split the train/val/test sets with 36,665, 9,508, and 5,410 samples, respectively.

ScanQA [39] is a large-scale dataset for 3D object-grounded question answering on point cloud. It consists of 41,363 questions and 58,191 answers, including 32,337 unique questions and

16,999 unique answers. Various types of questions in the dataset are collected through auto-generation and editing by humans. Alongside question-answer pairs, the dataset also includes 3D object localization annotations for 800 indoor 3D scenes of the ScanNet dataset. There are two test sets with and without object annotations in ScanQA dataset.

SQA3D [144] is the largest dataset of grounded 3D scene understanding with the human-annotated question-answering pairs. It comprises 20.4k descriptions of 6.8k unique situations collected from 650 ScanNet scenes and 33.4k questions about these situations. These questions examine a wide spectrum of reasoning capabilities for an intelligent agent, ranging from spatial relation comprehension to commonsense understanding, navigation, and multi-hop reasoning. The dataset is divided into three splits, with a total of 518/65/67 scenes and 11,723/1,550/1,652 targets across the train/val/test sets, respectively.

5.2 Evaluation Metrics

5.2.1 Evaluation Metrics on 3D Semantic Segmentation

For semantic segmentation of 3D point cloud, mean Intersection-over-Union (mIoU) is the most frequently used performance criteria, which is defined as $\frac{1}{C} \sum_{c=1}^C \frac{TP_c}{TP_c + FP_c + FN_c}$, where TP_c , FP_c , and FN_c correspond to the number of true positive, false positive, and false negative predictions for class c , and C is the number of classes. Besides, frequency-weighted IOU (FwIOU) is also used in 3D semantic segmentation, which is similar to mIoU except that each IoU is weighted by the point-level frequency of its class.

5.2.2 Evaluation Metrics on 3D Object Detection

Average Precision (AP) is the main evaluation metric used in 3D object detection, which is calculated as the area under the precision-recall curve [170]. Based on the original definition of AP, some dataset-specific evaluation metrics are developed for different datasets. For the KITTI dataset, Average Orientation Similarity (AOS) is introduced to assess the accuracy of orientation estimation [11]. For the nuScenes dataset, nuScenes detection score (NDS) is the major evaluation metric.

5.2.3 Evaluation Metrics on 3D Visual Grounding

In 3D VG, the evaluation metric is the $Acc@mIoU$, which means the fraction of descriptions whose predicted box overlaps the ground truth with $IoU > m$, where $m \in \{0.25, 0.5\}$ [37]. The accuracy is reported in unique and multiple categories, where a target object is classified as unique if it is the only object of its class in the scene. Otherwise, it is classified as multiple.

5.2.4 Evaluation Metrics on 3D Dense Captioning

For 3D dense captioning, the most commonly used evaluation metric is $m@kIoU$ [38], which enables a holistic assessment of both the quality of the generated descriptions and the detected bounding boxes. $m@kIoU$ is defined as $m@kIoU = \frac{1}{N} \sum_{i=0}^N m_i u_i$, where $u_i \in \{0, 1\}$ is set to 1 if the IoU score for the i^{th} box is greater than k , otherwise 0. In the metric, m represents the captioning metrics CIDEr [171], BLEU-4 [172], METEOR [173], and ROUGE [174], abbreviated as C, B-4, M, R, respectively. N is the number of ground truth or detected object bounding boxes.

TABLE 1

The 3D object detection results on KITTI in terms of mAP. Results of car, pedestrian, and cyclist are evaluated by mAP with the IoU threshold of 0.7, 0.5, and 0.5, respectively. Frustum-PointPillars and Faraway-Frustum are abbreviated to Frst-PointPillars and Faraway-Frst, respectively. Camera-LiDAR projection-based, attention mechanism-based and cross-modal Transformer-based methods are abbreviated to CLP-based, AM-based, and CMT-based methods, respectively.

Type	Method	Venue	Car				Pedestrian				Cyclist			
			Mod	Easy	Hard	mAP	Mod	Easy	Hard	mAP	Mod	Easy	Hard	mAP
CLP-based	PointPainting [47]	CVPR2020	71.70	82.11	67.08	73.63	40.97	50.32	37.87	45.65	63.78	77.63	55.89	65.77
	EPNet [48]	ECCV2020	79.28	89.81	74.59	81.23	-	-	-	-	-	-	-	-
	Frst-PointPillars [52]	ICCV2021	-	-	-	-	42.89	51.22	39.28	44.46	-	-	-	-
	Faraway-Frst [54]	ITSC2021	79.05	87.45	76.14	80.88	38.58	46.33	35.71	40.21	62.00	77.36	55.4	64.92
	EPNet++ [49]	TPAMI2022	81.96	91.37	76.71	83.35	44.38	52.79	41.29	46.15	59.71	76.15	53.67	63.18
AM-based	3D-CVF [66]	ECCV2020	80.05	89.20	73.11	80.79	-	-	-	-	-	-	-	-
	SFD [65]	CVPR2022	84.76	91.73	77.92	84.80	-	-	-	-	-	-	-	-
	PA3DNet [60]	TIH2023	82.57	90.49	77.88	83.65	-	-	-	-	-	-	-	-
	LoGoNet [69]	CVPR2023	85.06	91.80	80.74	85.87	47.43	53.07	45.22	48.57	71.70	84.47	64.67	73.61
CMT-based	CAT-Det [73]	CVPR2022	81.32	89.87	76.68	82.62	45.44	54.26	41.94	47.21	68.81	83.68	61.45	71.31

TABLE 2

The 3D object detection results on nuScenes. Camera-LiDAR projection-based, attention mechanism-based and cross-modal Transformer-based methods are abbreviated to CLP-based, AM-based, and CMT-based methods, respectively.

Type	Method	Venue	NDS	mAP
CLP-based	MVP [55]	NeurIPS2021	70.5	66.4
	PointAugmenting [50]	CVPR2021	71.0	66.8
	MSMDFusion [51]	CVPR2023	75.1	73.3
AM-based	3D-CVF [66]	ECCV2020	66.3	57.8
	AutoAlign [67]	IJCAI2022	70.4	64.6
	AutoAlignV2 [68]	ECCV2022	72.4	68.4
	BEVFusion [58]	NeurIPS2022	73.3	71.3
	SparseFusion [64]	arXiv2023	73.8	72.0
CMT-based	UVTR [78]	NeurIPS2022	71.1	67.1
	TransFusion [74]	CVPR2022	71.7	68.9
	LIFT [80]	CVPR2022	70.2	65.1
	FUTR3D [169]	CVPR2023	72.1	69.4
	CMT [75]	ICCV2023	77.0	75.3
	FocalFormer3D [77]	ICCV2023	74.5	72.4
	UniTR [79]	ICCV2023	74.5	70.9
	BEVFusion4D [81]	arXiv2023	77.2	76.8

TABLE 3

The 3D semantic segmentation results on SemanticKITTI and nuScenes. SemanticKITTI is abbreviated as S-KITTI. Interactive fusion-based and knowledge distillation-based methods are abbreviated as IF-based and KD-based methods, respectively.

Type	Method	Venue	S-KITTI mIoU	nuScenes mIoU	FwIoU
IF-based	PMF [43]	ICCV2021	-	77.0	89.0
	RPVNet [93]	ICCV2021	70.3	-	-
	MSeg3D [95]	CVPR2023	-	81.1	91.4
KD-based	2DPASS [97]	ECCV2022	72.9	77.8	89.7
	CMDFusion [98]	arXiv2023	71.6	80.8	90.3

5.2.5 Evaluation Metrics on 3D Question Answering

To evaluate the performance of 3D QA, some frequently used evaluation metrics are EM@1 and EM@10, where EM@ K represents the percentage of predictions in which the top K predicted answers exactly match any one of the ground-truth answers [175]. Additionally, some sentence evaluation metrics commonly used for 3D dense captioning, including BLEU [172], ROUGE, METEOR, CIDEr, and SPICE [176] are added to analyze the robust answer matching, as some questions have multiple possible answer expressions.

5.3 Performance Comparison of 3D+2D Scene Understanding Approaches

This section describes the performance evaluation results of current 3D object detection and semantic segmentation approaches. Tabs. 1 and 2 summarize the 3D object detection results achieved by current approaches on KITTI and nuScenes benchmarks, respectively. The main observations are presented as follows:

- The detection performance for cars, pedestrians, and cyclists significantly declines on hard levels when compared to easy and moderate ones, as shown in Tab. 1. This discrepancy is mainly because, at the hard level, foreground objects that only account for a minor percentage of the whole scene are usually small, remote, or occluded. Hence, the further improvement direction of 3D object detection approaches is largely derived from the accurate identification of hard level objects since the acceptable performance of detecting large objects near sensors. One promising solution is the local fusion strategy based on the attention mechanism, like SFD and LoGoNet, which can capture regional cross-sensor features and avoid negative effects from overwhelming background information.
- Simultaneously considering spatial and temporal cross-sensor information, like BEVFusion4D, is effective for 3D object detection, as shown in Tab. 2. On the one hand, historical location and orientation information of moving objects benefit their current motion estimation. On the other hand, temporal information can also help detect remote or occluded objects in the current time because of complementary cues encoded in adjacent frames. Notably, direct aggregating 4D spatiotemporal data, such as LIFT, may yield unsatisfactory performance. This is primarily because dense 4D representation inherently contains redundant information, which makes it more challenging to align objects across different sensors and timestamps. Hence, separation modeling of spatial-domain and temporal-domain, exemplified by BEVFusion4D, is a promising research direction.

Tab. 3 summarize the 3D semantic segmentation results achieved by current approaches. The results of unsupervised domain adaptation are omitted because of inconsistent experimental settings. The main observations are presented as follows:

TABLE 4

The 3D visual grounding results on ScanRefer in which accuracy is evaluated by Acc@0.25IoU and Acc@0.5IoU. Two-stage detect-then-match and one-stage language-guided methods are abbreviated to two-stage and one-stage methods, respectively. ‡ denotes joint grounding and captioning, or 3D vision-language pre-training methods.

Type	Method	Venue	Unique		Multiple		Overall	
			Acc@0.25	Acc@0.5	Acc@0.25	Acc@0.5	Acc@0.25	Acc@0.5
Two-stage	ScanRefer [37]	ECCV2020	67.64	46.19	32.06	21.26	38.97	26.10
	ReferIt3D [121]	ECCV2020	53.80	37.50	21.00	12.80	26.40	16.90
	TGNN [122]	AAAI2021	68.61	56.80	29.84	23.18	37.37	29.70
	InstanceRefer [124]	ICCV2021	77.45	66.83	31.27	24.77	40.23	32.93
	SAT [130]	ICCV2021	73.21	50.83	37.64	25.16	44.54	30.14
	FFL_3DOG [123]	ICCV2021	78.80	67.94	35.19	25.70	41.33	34.01
	3DVG-Transformer [127]	ICCV2021	77.16	58.47	38.38	28.70	45.90	34.47
	MVT [129]	CVPR2022	77.67	66.45	31.92	25.26	40.80	33.26
	3DJCG ‡ [166]	CVPR2022	78.75	61.30	40.13	30.08	47.62	36.14
	3DVLP ‡ [167]	CVPR2023	79.35	62.60	42.54	32.18	49.68	38.08
	3D-VisTA ‡ [32]	ICCV2023	81.60	75.10	43.70	39.10	50.60	45.80
One-stage	3D-SPS [112]	CVPR2022	81.63	64.77	39.48	29.61	47.65	36.43
	BUTD-DETR [133]	ECCV2022	82.88	64.98	44.73	33.97	50.42	38.60
	EDA [136]	CVPR2023	85.76	68.57	49.13	37.64	57.59	42.26

TABLE 5

The 3D dense captioning results on ScanRefer. Traditional captioning metrics, *i.e.*, CIDEr (C), BLEU-4 (B-4), METEOR (M), and ROUGE (R), are used for evaluation. Two stage detect-then-describe and one-stage parallel detect-describe methods are abbreviated to two-stage and one-stage methods, respectively.

Type	Method	Venue	IoU=0.25				IoU=0.50			
			C	B-4	M	R	C	B-4	M	R
Two-stage	Scan2Cap [38]	CVPR2021	53.73	34.25	26.14	54.95	35.20	22.36	21.44	43.57
	SpaCap3d [141]	IJCAI2022	58.06	35.30	26.16	55.03	42.76	25.38	22.84	45.66
	MORE [140]	ECCV2022	58.89	35.41	26.36	55.41	38.98	23.01	21.65	44.33
	3DJCG ‡ [166]	CVPR2022	60.86	39.67	27.45	59.02	47.68	31.53	24.28	51.80
	3DVLP ‡ [167]	CVPR2023	64.09	39.84	27.65	58.78	50.02	31.87	24.53	51.17
	3D-VisTA ‡ [32]	ICCV2023	71.00	36.50	28.40	57.60	66.90	34.00	27.10	54.30
One-stage	Vote2Cap-DETR [143]	CVPR2023	71.45	39.34	28.25	59.33	61.81	34.46	26.22	54.40

- For interactive fusion-based segmentation approaches, addressing the limited intersection on the FOV between sensors is important to improve the overall performance. This is because only 3D points falling into the intersected FOV are geometrically associated with 2D pixels, while only considering the intersected multi-modal data may discard a lot of useful information in those unmatched point-pixel pairs. Overcoming the inapplicable and overlooked LiDAR-camera fusion outside the sensor FOV intersection, like MSeg3D, can bring huge performance improvements. Inspired by MSeg3D, we believe that cross-modal feature completion and semantic-based feature fusion are promising directions to solve the above problem.
- Knowledge distillation-based segmentation approaches can achieve comparable performance to interactive fusion-based methods. Notably, interactive fusion-based methods conduct both training and inference using LiDAR and camera pairs, while knowledge distillation-based approaches are trained on the LiDAR and camera data but only require LiDAR modality during inference. Being free from camera modality during inference can bring two advantages. On the one hand, fewer computational resources are consumed because only point cloud data is required to process, reducing the burden on real-time applications. On the other hand, the limited intersection on the FOV between sensors can be solved to a certain extent via cross-modal knowledge distillation.

5.4 Performance Comparison of 3D+Language Scene Understanding Approaches

This section evaluates the performance of various recently proposed approaches for 3D+language scene understanding. Tabs. 4 and 5 summarize the 3D visual grounding and dense captioning results achieved by current approaches on the ScanRefer dataset. The main observations are presented as follows:

- In both 3D visual grounding and dense captioning, single-stage approaches (*e.g.*, BUTD-DETR, Vote2Cap-DETR, and EDA) demonstrate significantly superior performance compared to two-stage task-specific methods (*e.g.*, SAT, SpaCap3D, and 3DVG-Transformer). This is because single-stage methods overcome the limitations of reliance on the 3D detection backbone, *i.e.*, missing the target instance when proposals are sparse and facing difficulty in modeling spatial relationships when proposals are redundant.
- For two-stage approaches, unified frameworks for 3D visual grounding and dense captioning (*e.g.*, 3DJCG) yield better performance than other task-specific approaches. This highlights the importance of leveraging the complementary nature between 3D visual grounding and dense captioning, *i.e.*, relationships among objects learned by 3D visual grounding, and attributes of target object learned by 3D dense captioning.

Tabs. 6 and 7 summarizes the visual and situated 3D question answering performance achieved by current approaches on the

TABLE 6

The visual question answering results on ScanQA in terms of dense captioning metrics. “w/ objects” and “w/o objects” stand for whether the approach utilizes the 3D object detection as the auxiliary task. ‡ denotes joint grounding and captioning, or 3D vision-language pre-training methods.

Method	Venue	EM@1	EM@10	BLEU-1	BLEU-2	BLEU-3	BLEU-4	ROUGE	METEOR	CIDEr	SPICE
Test set w/ objects											
Scanrefer + MCAN [39]	CVPR2022	20.56	52.35	27.85	17.27	11.88	7.46	30.68	11.97	57.36	10.58
ScanQA w/o multiview [39]	CVPR2022	22.49	-	30.82	-	-	9.66	33.37	13.17	64.55	-
ScanQA [39]	CVPR2022	23.45	56.51	31.56	21.39	15.87	12.04	34.34	13.55	67.29	11.99
3DVLP ‡ [167]	CVPR2023	24.58	55.97	33.15	22.65	16.38	11.23	35.97	14.16	70.18	12.71
3D-VisTA ‡ [32]	ICCV2023	27.00	57.90	-	-	-	16.00	38.60	15.20	76.60	-
Test set w/o objects											
Scanrefer + MCAN [39]	CVPR2022	19.04	49.70	26.98	16.17	11.28	7.82	28.61	11.38	53.41	10.63
ScanQA w/o multiview [39]	CVPR2022	20.05	-	30.84	-	-	12.80	30.60	12.66	59.95	-
ScanQA [39]	CVPR2022	20.90	54.11	30.68	21.20	15.81	10.75	31.09	12.59	60.24	11.29
3DVLP ‡ [167]	CVPR2023	21.56	53.89	31.48	23.56	19.62	15.84	31.79	13.13	63.40	12.53
3D-VisTA ‡ [32]	ICCV2023	23.00	53.50	-	-	-	11.90	32.80	12.90	62.60	-

TABLE 7

The situated question answering results on SQA3D. “What”, “Is”, “How”, “Can”, “Which”, and “Others” represent the types of questions based on their prefixes. V=3D visual information S, S=situation description s^{txt} , Q=question, A=answer, L=location<position, rotation>. In ScanQA, aux. indicates the use of position and rotation as the auxiliary loss. ‡ denotes joint grounding and captioning, or 3D vision-language pre-training methods.

Method	Venue	\mathcal{S}	Format	test set						Avg.
				What	Is	How	Can	Which	Others	
Blind test		-	SQ→A	26.75	63.34	43.44	69.53	37.89	43.41	43.65
ScanQA(w/o s^{txt}) [39]	CVPR2022	3D scan	VQ→A	28.58	65.03	47.31	66.27	43.87	42.88	45.27
ScanQA [144]	ICLR2022	3D scan	VSQ→A	31.64	63.80	46.02	69.53	43.87	45.34	46.58
SQA3D [144]	ICLR2022	3D scan	VSQ→AL	33.48	66.10	42.37	69.53	43.02	46.40	47.20
3D-VisTA ‡ [32]	ICCV2023	3D scan	VSQ→AL	34.80	63.30	45.40	69.80	47.20	48.10	48.50
Unified QA _{large} [146]	EMNLP2020	ScanRefer	VSQ→A	33.01	50.43	31.91	56.51	45.17	41.11	41.00
Unified QA _{large} [146]	EMNLP2020	ReferIt3D	VSQ→A	27.58	47.99	34.05	59.47	40.91	39.77	38.71
GPT-3 [145]	NeurIPS2020	ScanRefer	VAQ→A	39.67	45.99	40.47	45.56	36.08	38.42	41.00
GPT-3 [145]	NeurIPS2020	ReferIt3D	VSQ→A	28.90	46.42	28.05	40.24	30.11	36.07	34.57
Human(amateur)		3D scan	VSQ→A	88.53	93.84	88.44	95.27	87.22	88.57	90.06

ScanQA and SQA3D datasets, respectively. The main observations are presented as follows:

- On the ScanQA dataset, 3D-VisTA and 3DVLP significantly outperform other visual question answering approaches. Similarly, when evaluated on the SQA3D dataset, 3D-VisTA performs better than other situated question answering methods. These phenomena confirm the effectiveness of 3D-language pre-training approaches on 3D question answering, largely stemming from the geometry information modeling and scene-language alignment. On the one hand, geometry information modeling is helpful in calculating distance, angle, and direction between different instances, enhancing the performance of spatial relationship reasoning. On the other hand, scene-language alignment can match object names mentioned in the question with object instances in the scene.
- For more complex 3D situated question answering, as depicted in Tab. 7, removing the input situation description and the auxiliary situation prediction loss causes worse results, especially on the “What” questions. This is because ignoring the situation that the question depends on makes the model more vulnerable to unrelated answers. For example, “What is behind of me” may have various answers under situations from different first-person perspectives. Besides, the powerful Unified QA and GPT-3 fail to generate reasonable answers, mainly because of the bottleneck of the 3D captions, *i.e.*, scene captions

from point clouds only contain insufficient and incomplete geometry information.

6 CONCLUSION AND OUTLOOKS

This survey offers an in-depth look at the latest in multimodal 3D scene understanding. We commenced by summarizing the task definitions and challenges intrinsic to 3D+2D and 3D+language cases. This was followed by a structured taxonomy of pivotal techniques for each task. Moreover, we provided comparative results of recent advances on several benchmark datasets, together with insightful observation. Our aspiration is for this survey to serve as a comprehensive guide for newcomers and seasoned practitioners alike. There are still numerous possibilities for further exploration into multi-modal 3D scene understanding. Some promising future research directions are provided in the following.

Large-scale 3D-language foundational model. Current 3D VLMs based on 2D-to-3D transfer are limited in zero-shot capabilities and downstream applications, largely due to the restricted scale of data and inadequate preservation of geometry [41]. This underscores the imperative for a large-scale 3D-language foundational model. The primary solution to address this challenge lies in the creation of large dataset that can support the training of VLMs from scratch. Additionally, efficient transfer learning methods, including techniques like prompt tuning [177] and LORA [178], hold great promise in enhancing practical applicability by leveraging pre-trained knowledge for specific tasks.

Data-efficient training. Given the significant cost associated with data collection and annotation, much of the current research is limited to small-scale datasets. As a result, there is an increasing need to emphasize the development of robust model training and optimization tailored for limited data, thereby reducing the dependency on extensive datasets. Recent studies have exhibited promising results in addressing data annotation challenges through unsupervised and weakly-supervised learning approaches. Besides, synthesizing realistic samples using text-to-image or text-to-3D generation is expected to be further investigated, which potentially alleviates data collection issue.

Computational efficiency of 3D modeling. Given the substantial volume of point cloud, computational demands can escalate significantly. As such, computationally efficient 3D models become imperative. To address this challenge, adopting model compression techniques, such as quantization [179], pruning [180], and efficient structures [181], are essential to diminish computation complexity. Moreover, leveraging hardware optimization like Flash attention [182] can facilitate the deployment of applications on edge devices, offering another avenue for enhanced efficiency.

Incorporation of additional modalities. Although impressive progress has been observed in multimodal 3D modeling, the predominant emphasis is still on image and language. We envisage the incorporation of further modalities, such as audio, into a consolidated model to fit their joint distributions, which is more helpful to understand complex 3D scenes. Given the intricate training requirements and the scarcity of paired data when training a new model, it might be more effective to enhance existing multimodal 3D models by integrating additional modalities. A viable approach [183] is to align each well-posed, modality-specific model using a minimal set of paired data.

ACKNOWLEDGMENTS

This work was supported by the National Natural Science Foundation of China (No.62276176).

REFERENCES

- [1] Y. Zeng, C. Jiang, J. Mao, J. Han, C. Ye, Q. Huang, D. Y. Yeung, Z. Yang, X. Liang, and H. Xu, "CLIP²: Contrastive language-image-point pretraining from real-world point cloud data," in *CVPR*, 2023, pp. 15 244–15 253. [1](#)
- [2] Y. Yang, M. Hayat, Z. Jin, H. Zhu, and Y. Lei, "Zero-shot point cloud segmentation by semantic-visual aware synthesis," in *ICCV*, 2023, pp. 11 586–11 596. [1](#)
- [3] Y. Yang, M. Hayat, Z. Jin, C. Ren, and Y. Lei, "Geometry and uncertainty-aware 3D point cloud class-incremental semantic segmentation," in *CVPR*, 2023, pp. 21 759–21 768. [1](#)
- [4] V. Mittal, "Attngrinder: Talking to cars with attention," in *ECCV*, 2020, pp. 62–73. [1](#)
- [5] X. Wang, Q. Huang, A. Celikyilmaz, J. Gao, D. Shen, Y.-F. Wang, W. Y. Wang, and L. Zhang, "Reinforced cross-modal matching and self-supervised imitation learning for vision-language navigation," in *CVPR*, 2019, pp. 6629–6638. [1](#)
- [6] C. Bermejo, L. H. Lee, P. Chojecki, D. Przewozny, and P. Hui, "Exploring button designs for mid-air interaction in virtual reality: A hexa-metric evaluation of key representations and multi-modal cues," *ACM HCI*, vol. 5, pp. 1–26, 2021. [1](#)
- [7] I. Armeni, O. Sener, A. R. Zamir, H. Jiang, I. Brilakis, M. Fischer, and S. Savarese, "3D semantic parsing of large-scale indoor spaces," in *CVPR*, 2016, pp. 1534–1543. [1](#)
- [8] A. Dai, A. X. Chang, M. Savva, M. Halber, T. Funkhouser, and M. Nießner, "ScanNet: Richly-annotated 3D reconstructions of indoor scenes," in *CVPR*, 2017, pp. 5828–5839. [1](#), [12](#), [13](#)
- [9] N. Silberman, D. Hoiem, P. Kohli, and R. Fergus, "Indoor segmentation and support inference from rgbd images," in *ECCV*, 2012, pp. 746–760. [1](#)
- [10] Z. Jin, Y. Lei, N. Akhtar, H. Li, and M. Hayat, "Deformation and correspondence aware unsupervised synthetic-to-real scene flow estimation for point clouds," in *CVPR*, 2022, pp. 7233–7243. [1](#)
- [11] A. Geiger, P. Lenz, and R. Urtasun, "Are we ready for autonomous driving? the kitti vision benchmark suite," in *CVPR*, 2012, pp. 3354–3361. [1](#), [13](#)
- [12] Y. Guo, H. Wang, Q. Hu, H. Liu, L. Liu, and M. Bennamoun, "Deep learning for 3D point clouds: A survey," *IEEE TPAMI*, vol. 43, no. 12, pp. 4338–4364, 2020. [1](#)
- [13] J. Zhuangwei, G. Haiyan, Z. Yufu, N. Huan, L. Dilong, and Y. Yongtao, "Survey of point cloud semantic segmentation based on deep learning," *JCST*, vol. 15, no. 1, p. 1, 2021. [1](#)
- [14] W. Zimmer, E. Ercelik, X. Zhou, X. J. D. Ortiz, and A. Knoll, "A survey of robust 3d object detection methods in point clouds," *arXiv preprint arXiv:2204.00106*, 2022. [1](#)
- [15] Z. Zhou, Y. Lei, B. Zhang, L. Liu, and Y. Liu, "ZegCLIP: Towards adapting clip for zero-shot semantic segmentation," in *CVPR*, 2023, pp. 11 175–11 185. [1](#)
- [16] D. J. Yeong, V. H. Gustavo, J. Barry, and J. Walsh, "Sensor and sensor fusion technology in autonomous vehicles: A review," *Sensors*, vol. 21, no. 6, p. 2140, 2021. [1](#)
- [17] X. Li, Y. Xiao, B. Wang, H. Ren, Y. Zhang, and J. Ji, "Automatic targetless LiDAR-camera calibration: a survey," *AIR*, vol. 56, no. 9, pp. 9949–9987, 2023. [1](#)
- [18] Z. Zhang, Z. Zhang, Q. Yu, R. Yi, Y. Xie, and L. Ma, "LiDAR-camera panoptic segmentation via geometry-consistent and semantic-aware alignment," in *ICCV*, 2023, pp. 3662–3671. [1](#)
- [19] L. Xie, C. Xiang, Z. Yu, G. Xu, Z. Yang, D. Cai, and X. He, "PI-RCNN: An efficient multi-sensor 3D object detector with point-based attentive cont-conv fusion module," in *AAAI*, vol. 34, no. 07, 2020, pp. 12 460–12 467. [1](#)
- [20] S. Xu, D. Zhou, J. Fang, J. Yin, Z. Bin, and L. Zhang, "FusionPainting: Multimodal fusion with adaptive attention for 3D object detection," in *ITSC*, 2021, pp. 3047–3054. [1](#)
- [21] H. Zhu, J. Deng, Y. Zhang, J. Ji, Q. Mao, H. Li, and Y. Zhang, "VPFNet: Improving 3D object detection with virtual point based lidar and stereo data fusion," *IEEE TMM*, 2022. [1](#)
- [22] C. R. Qi, H. Su, K. Mo, and L. J. Guibas, "PointNet: Deep learning on point sets for 3D classification and segmentation," in *CVPR*, 2017, pp. 652–660. [1](#)
- [23] C. R. Qi, L. Yi, H. Su, and L. J. Guibas, "PointNet++: Deep hierarchical feature learning on point sets in a metric space," in *NeurIPS*, vol. 30, 2017. [1](#)
- [24] C. R. Qi, O. Litany, K. He, and L. J. Guibas, "Deep hough voting for 3D object detection in point clouds," in *ICCV*, 2019, pp. 9277–9286. [1](#), [6](#)
- [25] C. Choy, J. Gwak, and S. Savarese, "4D Spatio-Temporal ConvNets: Minkowski convolutional neural networks," in *CVPR*, 2019, pp. 3075–3084. [1](#)
- [26] M. Joseph-Rivlin, A. Zvirin, and R. Kimmel, "Momen (e) t: Flavor the moments in learning to classify shapes," in *ICCVW*, 2019, pp. 1–10. [1](#)
- [27] H. Zhao, L. Jiang, J. Jia, P. H. Torr, and V. Koltun, "Point Transformer," in *ICCV*, 2021, pp. 16 259–16 268. [1](#)
- [28] Z. Lin, X. Peng, P. Cong, Y. Hou, X. Zhu, S. Yang, and Y. Ma, "WildRefer: 3D object localization in large-scale dynamic scenes with multi-modal visual data and natural language," *arXiv preprint arXiv:2304.05645*, 2023. [1](#)
- [29] J. Hsu, J. Mao, and J. Wu, "NS3D: Neuro-symbolic grounding of 3D objects and relations," in *CVPR*, 2023, pp. 2614–2623. [1](#)
- [30] Y. Qiu, S. Yamamoto, R. Yamada, R. Suzuki, H. Kataoka, K. Iwata, and Y. Satoh, "3D change localization and captioning from dynamic scans of indoor scenes," in *WACV*, 2023, pp. 1176–1185. [1](#)
- [31] Z. Wang, H. Huang, Y. Zhao, L. Li, X. Cheng, Y. Zhu, A. Yin, and Z. Zhao, "Distilling coarse-to-fine semantic matching knowledge for weakly supervised 3D visual grounding," in *ICCV*, 2023, pp. 2662–2671. [1](#)
- [32] Z. Zhu, X. Ma, Y. Chen, Z. Deng, S. Huang, and Q. Li, "3D-VisTA: Pre-trained transformer for 3D vision and text alignment," in *ICCV*, 2023, pp. 2911–2921. [1](#), [12](#), [15](#), [16](#)
- [33] H. Senior, G. Slabaugh, S. Yuan, and L. Rossi, "Graph neural networks in vision-language image understanding: A survey," *arXiv preprint arXiv:2303.03761*, 2023. [1](#)
- [34] W. Jin, Z. Zhao, X. Cao, J. Zhu, X. He, and Y. Zhuang, "Adaptive spatio-temporal graph enhanced vision-language representation for video QA," *IEEE TIP*, vol. 30, pp. 5477–5489, 2021. [1](#)

- [35] Y. Wang, Q. Mao, H. Zhu, J. Deng, Y. Zhang, J. Ji, H. Li, and Y. Zhang, “Multi-modal 3D object detection in autonomous driving: a survey,” *IJCV*, pp. 1–31, 2023. [2](#)
- [36] D. Peng, Y. Lei, M. Hayat, Y. Guo, and W. Li, “Semantic-aware domain generalized segmentation,” in *CVPR*, 2022, pp. 2594–2605. [2](#)
- [37] D. Z. Chen, A. X. Chang, and M. Nießner, “ScanRefer: 3D object localization in RGB-D scans using natural language,” in *ECCV*, 2020, pp. 202–221. [2](#), [8](#), [13](#), [15](#)
- [38] Z. Chen, A. Gholami, M. Nießner, and A. X. Chang, “Scan2cap: Context-aware dense captioning in RGB-D scans,” in *CVPR*, 2021, pp. 3193–3203. [2](#), [10](#), [13](#), [15](#)
- [39] D. Azuma, T. Miyanishi, S. Kurita, and M. Kawanabe, “ScanQA: 3D question answering for spatial scene understanding,” in *CVPR*, 2022, pp. 19 129–19 139. [2](#), [3](#), [11](#), [13](#), [16](#)
- [40] C. Li, C. Zhang, A. Waghware, L. H. Lee, F. Rameau, Y. Yang, S. H. Bae, and C. S. Hong, “Generative AI meets 3D: A survey on text-to-3D in AIGC era,” *arXiv preprint arXiv:2305.06131*, 2023. [2](#)
- [41] R. Ding, J. Yang, C. Xue, W. Zhang, S. Bai, and X. Qi, “PLA: Language-driven open-vocabulary 3D scene understanding,” in *CVPR*, 2023, pp. 7010–7019. [2](#), [16](#)
- [42] C. R. Qi, X. Chen, O. Litany, and L. J. Guibas, “ImVoteNet: Boosting 3D object detection in point clouds with image votes,” in *CVPR*, 2020, pp. 4404–4413. [3](#), [6](#)
- [43] Z. Zhuang, R. Li, K. Jia, Q. Wang, Y. Li, and M. Tan, “Perception-aware multi-sensor fusion for 3D LiDAR semantic segmentation,” in *ICCV*, 2021, pp. 16 280–16 290. [3](#), [7](#), [8](#), [14](#)
- [44] D. Z. Chen, R. Hu, X. Chen, M. Nießner, and A. X. Chang, “UniT3D: A unified transformer for 3D dense captioning and visual grounding,” *arXiv preprint arXiv:2212.00836*, 2022. [3](#)
- [45] D. Z. Chen, Q. Wu, M. Nießner, and A. X. Chang, “D3Net: A unified speaker-listener architecture for 3D dense captioning and visual grounding,” in *ECCV*, 2022, pp. 487–505. [3](#), [12](#)
- [46] J. Dou, J. Xue, and J. Fang, “SEG-VoxelNet for 3D vehicle detection from RGB and LiDAR data,” in *ICRA*, 2019, pp. 4362–4368. [3](#)
- [47] S. Vora, A. H. Lang, B. Helou, and O. Beijbom, “PointPainting: Sequential fusion for 3D object detection,” in *CVPR*, 2020, pp. 4604–4612. [4](#), [14](#)
- [48] T. Huang, Z. Liu, X. Chen, and X. Bai, “EPNet: Enhancing point features with image semantics for 3D object detection,” in *ECCV*, 2020, pp. 35–52. [4](#), [14](#)
- [49] Z. Liu, T. Huang, B. Li, X. Chen, X. Wang, and X. Bai, “EPNet++: Cascade bi-directional fusion for multi-modal 3D object detection,” *IEEE TPAMI*, 2022. [4](#), [14](#)
- [50] C. Wang, C. Ma, M. Zhu, and X. Yang, “PointAugmenting: Cross-modal augmentation for 3D object detection,” in *CVPR*, 2021, pp. 11 794–11 803. [4](#), [14](#)
- [51] Y. Jiao, Z. Jie, S. Chen, J. Chen, L. Ma, and Y. G. Jiang, “MSMDfusion: Fusing lidar and camera at multiple scales with multi-depth seeds for 3D object detection,” in *CVPR*, 2023, pp. 21 643–21 652. [4](#), [14](#)
- [52] A. Paigwar, D. Sierra-Gonzalez, Ö. Erkent, and C. Laugier, “Frustum-PointPillars: A multi-stage approach for 3D object detection using RGB camera and LiDAR,” in *ICCV*, 2021, pp. 2926–2933. [4](#), [14](#)
- [53] A. H. Lang, S. Vora, H. Caesar, L. Zhou, J. Yang, and O. Beijbom, “PointPillars: Fast encoders for object detection from point clouds,” in *CVPR*, 2019, pp. 12 697–12 705. [4](#)
- [54] H. Zhang, D. Yang, E. Yurtsever, K. A. Redmill, and Ü. Özgüner, “Faraway-Frustum: Dealing with LiDAR sparsity for 3D object detection using fusion,” in *ITSC*, 2021, pp. 2646–2652. [4](#), [14](#)
- [55] T. Yin, X. Zhou, and P. Krähenbühl, “Multimodal virtual point 3D detection,” in *NeurIPS*, vol. 34, 2021, pp. 16 494–16 507. [4](#), [14](#)
- [56] Y. Liu, O. Yoshie, and H. Watanabe, “Application of multi-modal fusion attention mechanism in semantic segmentation,” in *ACCV*, 2022, pp. 1245–1264. [4](#)
- [57] M. Korban, P. Youngs, and S. T. Acton, “A multi-modal transformer network for action detection,” *PR*, vol. 142, p. 109713, 2023. [4](#)
- [58] T. Liang, H. Xie, K. Yu, Z. Xia, Z. Lin, Y. Wang, T. Tang, B. Wang, and Z. Tang, “BEVFusion: A simple and robust LiDAR-camera fusion framework,” in *NeurIPS*, vol. 35, 2022, pp. 10 421–10 434. [4](#), [14](#)
- [59] J. Hu, L. Shen, and G. Sun, “Squeeze-and-Excitation Networks,” in *CVPR*, 2018, pp. 7132–7141. [5](#)
- [60] M. Wang, L. Zhao, and Y. Yue, “PA3DNet: 3D vehicle detection with pseudo shape segmentation and adaptive camera-LiDAR fusion,” *TII*, 2023. [5](#), [14](#)
- [61] Y. Li, A. W. Yu, T. Meng, B. Caine, J. Ngiam, D. Peng, J. Shen, Y. Lu, D. Zhou, Q. V. Le *et al.*, “DeepFusion: LiDAR-camera deep fusion for multi-modal 3D object detection,” in *CVPR*, 2022, pp. 17 182–17 191. [5](#)
- [62] X. Chen, H. Ma, J. Wan, B. Li, and T. Xia, “Multi-view 3D object detection network for autonomous driving,” in *CVPR*, 2017, pp. 1907–1915. [5](#)
- [63] J. Ku, M. Mozifian, J. Lee, A. Harakeh, and S. L. Waslander, “Joint 3D proposal generation and object detection from view aggregation,” in *IROS*, 2018, pp. 1–8. [5](#)
- [64] Y. Xie, C. Xu, M.-J. Rakotosaona, P. Rim, F. Tombari, K. Keutzer, M. Tomizuka, and W. Zhan, “SparseFusion: Fusing multi-modal sparse representations for multi-sensor 3D object detection,” *arXiv preprint arXiv:2304.14340*, 2023. [5](#), [14](#)
- [65] X. Wu, L. Peng, H. Yang, L. Xie, C. Huang, C. Deng, H. Liu, and D. Cai, “Sparse fuse dense: Towards high quality 3D detection with depth completion,” in *CVPR*, 2022, pp. 5418–5427. [5](#), [14](#)
- [66] J. H. Yoo, Y. Kim, J. Kim, and J. W. Choi, “3D-CVF: Generating joint camera and LiDAR features using cross-view spatial feature fusion for 3D object detection,” in *ECCV*, 2020, pp. 720–736. [5](#), [14](#)
- [67] Z. Chen, Z. Li, S. Zhang, L. Fang, Q. Jiang, F. Zhao, B. Zhou, and H. Zhao, “AutoAlign: pixel-instance feature aggregation for multi-modal 3D object detection,” *arXiv preprint arXiv:2201.06493*, 2022. [5](#), [14](#)
- [68] Z. Chen, Z. Li, S. Zhang, L. Fang, Q. Jiang, and F. Zhao, “AutoAlignV2: Deformable feature aggregation for dynamic multi-modal 3D object detection,” *arXiv preprint arXiv:2207.10316*, 2022. [5](#), [14](#)
- [69] X. Li, T. Ma, Y. Hou, B. Shi, Y. Yang, Y. Liu, X. Wu, Q. Chen, Y. Li, Y. Qiao *et al.*, “LoGoNet: Towards accurate 3D object detection with local-to-global cross-modal fusion,” in *CVPR*, 2023, pp. 17 524–17 534. [5](#), [14](#)
- [70] Y. Shen, L. Wang, and Y. Jin, “AAFormer: a multi-modal transformer network for aerial agricultural images,” in *CVPR*, 2022, pp. 1705–1711. [5](#)
- [71] N. Shvetsova, B. Chen, A. Rouditchenko, S. Thomas, B. Kingsbury, R. S. Feris, D. Harwath, J. Glass, and H. Kuehne, “Everything at once: multi-modal fusion transformer for video retrieval,” in *CVPR*, 2022, pp. 20 020–20 029. [5](#)
- [72] X. Zhu, J. Zhu, H. Li, X. Wu, H. Li, X. Wang, and J. Dai, “Uni-Perceiver: Pre-training unified architecture for generic perception for zero-shot and few-shot tasks,” in *CVPR*, 2022, pp. 16 804–16 815. [5](#)
- [73] Y. Zhang, J. Chen, and D. Huang, “CAT-Det: Contrastively augmented transformer for multi-modal 3D object detection,” in *CVPR*, 2022, pp. 908–917. [5](#), [14](#)
- [74] X. Bai, Z. Hu, X. Zhu, Q. Huang, Y. Chen, H. Fu, and C. L. Tai, “TransFusion: Robust LiDAR-camera fusion for 3D object detection with transformers,” in *CVPR*, 2022, pp. 1090–1099. [5](#), [14](#)
- [75] J. Yan, Y. Liu, J. Sun, F. Jia, S. Li, T. Wang, and X. Zhang, “Cross modal transformer: Towards fast and robust 3D object detection,” in *ICCV*, 2023, pp. 18 268–18 278. [5](#), [14](#)
- [76] Y. Liu, T. Wang, X. Zhang, and J. Sun, “PETR: Position embedding transformation for multi-view 3D object detection,” in *ECCV*, 2022, pp. 531–548. [5](#)
- [77] Y. Chen, Z. Yu, Y. Chen, S. Lan, A. Anandkumar, J. Jia, and J. M. Alvarez, “FocalFormer3D: Focusing on hard instance for 3D object detection,” in *ICCV*, 2023, pp. 8394–8405. [5](#), [14](#)
- [78] Y. Li, Y. Chen, X. Qi, Z. Li, J. Sun, and J. Jia, “Unifying voxel-based representation with transformer for 3D object detection,” in *NeurIPS*, vol. 35, 2022, pp. 18 442–18 455. [5](#), [14](#)
- [79] H. Wang, H. Tang, S. Shi, A. Li, Z. Li, B. Schiele, and L. Wang, “UniTR: A unified and efficient multi-modal transformer for bird’s-eye-view representation,” in *ICCV*, 2023, pp. 6792–6802. [5](#), [14](#)
- [80] Y. Zeng, D. Zhang, C. Wang, Z. Miao, T. Liu, X. Zhan, D. Hao, and C. Ma, “LIFT: Learning 4D LiDAR image fusion transformer for 3D object detection,” in *CVPR*, 2022, pp. 17 172–17 181. [6](#), [14](#)
- [81] H. Cai, Z. Zhang, Z. Zhou, Z. Li, W. Ding, and J. Zhao, “BEV-Fusion4D: Learning LiDAR-camera fusion under bird’s-eye-view via cross-modality guidance and temporal aggregation,” *arXiv preprint arXiv:2303.17099*, 2023. [6](#), [14](#)
- [82] N. Carion, F. Massa, G. Synnaeve, N. Usunier, A. Kirillov, and S. Zagoruyko, “End-to-end object detection with transformers,” in *ECCV*, 2020, pp. 213–229. [6](#)
- [83] X. Zhu, W. Su, L. Lu, B. Li, X. Wang, and J. Dai, “Deformable DETR: Deformable transformers for end-to-end object detection,” *arXiv preprint arXiv:2010.04159*, 2020. [6](#)
- [84] X. Pan, Z. Xia, S. Song, L. E. Li, and G. Huang, “3D object detection with pointformer,” in *CVPR*, 2021, pp. 7463–7472. [6](#), [8](#)
- [85] T. Guan, J. Wang, S. Lan, R. Chandra, Z. Wu, L. Davis, and D. Manocha, “M3DeTR: Multi-representation, multi-scale, mutual-relation 3D object detection with transformers,” in *WACV*, 2022, pp. 772–782. [6](#)

- [86] Y. Wang, T. Ye, L. Cao, W. Huang, F. Sun, F. He, and D. Tao, "Bridged transformer for vision and point cloud 3D object detection," in *CVPR*, 2022, pp. 12 114–12 123. [6](#)
- [87] Y. Wang, X. Chen, L. Cao, W. Huang, F. Sun, and Y. Wang, "Multimodal token fusion for vision transformers," in *CVPR*, 2022, pp. 12 186–12 195. [6](#)
- [88] G. P. Meyer, J. Charland, D. Hegde, A. Laddha, and C. Vallespi-Gonzalez, "Sensor fusion for joint 3D object detection and semantic segmentation," in *CVPRW*, 2019, pp. 1–8. [6](#)
- [89] G. P. Meyer, A. Laddha, E. Kee, C. Vallespi-Gonzalez, and C. K. Wellington, "LaserNet: An efficient probabilistic 3D object detector for autonomous driving," in *CVPR*, 2019, pp. 12 677–12 686. [7](#)
- [90] G. Krispel, M. Opitz, G. Waltner, H. Possegger, and H. Bischof, "FuseSeg: LiDAR point cloud segmentation fusing multi-modal data," in *WACV*, 2020, pp. 1874–1883. [7](#)
- [91] M. Sandler, A. Howard, M. Zhu, A. Zhmoginov, and L. C. Chen, "MobileNetV2: Inverted residuals and linear bottlenecks," in *CVPR*, 2018, pp. 4510–4520. [7](#)
- [92] B. Wu, A. Wan, X. Yue, and K. Keutzer, "SqueezeSeg: Convolutional neural nets with recurrent CRF for real-time road-object segmentation from 3D LiDAR point cloud," in *ICRA*, 2018, pp. 1887–1893. [7](#)
- [93] J. Xu, R. Zhang, J. Dou, Y. Zhu, J. Sun, and S. Pu, "RPVNet: A deep and efficient range-point-voxel fusion network for LiDAR point cloud segmentation," in *ICCV*, 2021, pp. 16024–16033. [7](#), [14](#)
- [94] L. Zhao, H. Zhou, X. Zhu, X. Song, H. Li, and W. Tao, "LIF-Seg: LiDAR and camera image fusion for 3D lidar semantic segmentation," *IEEE TMM*, 2023. [7](#)
- [95] J. Li, H. Dai, H. Han, and Y. Ding, "Mseg3d: Multi-modal 3d semantic segmentation for autonomous driving," in *CVPR*, 2023, pp. 21 694–21 704. [7](#), [14](#)
- [96] J. Behley, M. Garbade, A. Milioto, J. Quenzel, S. Behnke, C. Stachniss, and J. Gall, "SemanticKITTI: A dataset for semantic scene understanding of LiDAR sequences," in *ICCV*, 2019, pp. 9297–9307. [7](#), [13](#)
- [97] X. Yan, J. Gao, C. Zheng, C. Zheng, R. Zhang, S. Cui, and Z. Li, "2DPASS: 2D priors assisted semantic segmentation on LiDAR point clouds," in *ECCV*, 2022, pp. 677–695. [7](#), [14](#)
- [98] J. Cen, S. Zhang, Y. Pei, K. Li, H. Zheng, M. Luo, Y. Zhang, and Q. Chen, "CMDFusion: Bidirectional fusion network with cross-modality knowledge distillation for LIDAR semantic segmentation," *arXiv preprint arXiv:2307.04091*, 2023. [7](#), [14](#)
- [99] M. Wang and W. Deng, "Deep visual domain adaptation: A survey," *Neurocomputing*, vol. 312, pp. 135–153, 2018. [7](#)
- [100] L. Yi, B. Gong, and T. Funkhouser, "Complete and label: A domain adaptation approach to semantic segmentation of LiDAR point clouds," in *CVPR*, 2021, pp. 15 363–15 373. [7](#)
- [101] R. Ding, J. Yang, L. Jiang, and X. Qi, "DODA: Data-oriented sim-to-real domain adaptation for 3D semantic segmentation," in *ECCV*, 2022, pp. 284–303. [7](#)
- [102] M. Jaritz, T. H. Vu, R. d. Charette, E. Wirbel, and P. Pérez, "xMUDA: Cross-modal unsupervised domain adaptation for 3D semantic segmentation," in *CVPR*, 2020, pp. 12 605–12 614. [7](#)
- [103] M. Jaritz, T. H. Vu, R. De Charette, É. Wirbel, and P. Pérez, "Cross-modal learning for domain adaptation in 3D semantic segmentation," *IEEE TPAMI*, vol. 45, no. 2, pp. 1533–1544, 2022. [7](#)
- [104] A. Cardace, P. Z. Ramirez, S. Salti, and L. Di Stefano, "Exploiting the complementarity of 2D and 3D networks to address domain-shift in 3D semantic segmentation," in *CVPR*, 2023, pp. 98–109. [8](#)
- [105] D. Peng, Y. Lei, W. Li, P. Zhang, and Y. Guo, "Sparse-to-dense feature matching: Intra and inter domain cross-modal learning in domain adaptation for 3D semantic segmentation," in *ICCV*, 2021, pp. 7108–7117. [8](#)
- [106] J. Dai, H. Qi, Y. Xiong, Y. Li, G. Zhang, H. Hu, and Y. Wei, "Deformable convolutional networks," in *ICCV*, 2017, pp. 764–773. [8](#)
- [107] A. Dai and M. Nießner, "3DMV: Joint 3D-multi-view prediction for 3D semantic scene segmentation," in *Proceedings of the ECCV*, 2018, pp. 452–468. [8](#)
- [108] J. Hou, A. Dai, and M. Nießner, "3D-SIS: 3D semantic instance segmentation of RGB-D scans," in *CVPR*, 2019, pp. 4421–4430. [8](#)
- [109] M. Jaritz, J. Gu, and H. Su, "Multi-view pointnet for 3D scene understanding," in *ICCVW*, 2019, pp. 1–9. [8](#)
- [110] W. Hu, H. Zhao, L. Jiang, J. Jia, and T.-T. Wong, "Bidirectional projection network for cross dimension scene understanding," in *CVPR*, 2021, pp. 14 373–14 382. [8](#)
- [111] D. Robert, B. Vallet, and L. Landrieu, "Learning multi-view aggregation in the wild for large-scale 3D semantic segmentation," in *CVPR*, 2022, pp. 5575–5584. [8](#)
- [112] J. Luo, J. Fu, X. Kong, C. Gao, H. Ren, H. Shen, H. Xia, and S. Liu, "3D-SPS: Single-stage 3D visual grounding via referred point progressive selection," in *CVPR*, 2022, pp. 16 454–16 463. [9](#), [15](#)
- [113] C. Zhu, Y. Zhou, Y. Shen, G. Luo, X. Pan, M. Lin, C. Chen, L. Cao, X. Sun, and R. Ji, "SeqTR: A simple yet universal network for visual grounding," in *ECCV*, 2022, pp. 598–615. [8](#)
- [114] L. Yang, Y. Xu, C. Yuan, W. Liu, B. Li, and W. Hu, "Improving visual grounding with visual-linguistic verification and iterative reasoning," in *CVPR*, 2022, pp. 9499–9508. [8](#)
- [115] H. Jiang, Y. Lin, D. Han, S. Song, and G. Huang, "Pseudo-Q: Generating pseudo language queries for visual grounding," in *CVPR*, 2022, pp. 15 513–15 523. [8](#)
- [116] Y. Zhou and O. Tuzel, "VoxelNet: End-to-end learning for point cloud based 3D object detection," in *CVPR*, 2018, pp. 4490–4499. [8](#)
- [117] C. He, H. Zeng, J. Huang, X.-S. Hua, and L. Zhang, "Structure aware single-stage 3D object detection from point cloud," in *CVPR*, 2020, pp. 11 873–11 882. [8](#)
- [118] F. Engelmann, T. Kontogianni, A. Hermans, and B. Leibe, "Exploring spatial context for 3D semantic segmentation of point clouds," in *ICCVW*, 2017, pp. 716–724. [8](#)
- [119] F. Engelmann, T. Kontogianni, J. Schult, and B. Leibe, "Know what your neighbors do: 3D semantic segmentation of point clouds," in *ECCV*, 2019, pp. 395–409. [8](#)
- [120] Y. Xie, J. Tian, and X. X. Zhu, "Linking points with labels in 3D: A review of point cloud semantic segmentation," *IEEE GRSM*, vol. 8, no. 4, pp. 38–59, 2020. [8](#)
- [121] P. Achlioptas, A. Abdelreheem, F. Xia, M. Elhoseiny, and L. Guibas, "ReferIt3D: Neural listeners for fine-grained 3D object identification in real-world scenes," in *ECCV*, 2020, pp. 422–440. [8](#), [15](#)
- [122] P. H. Huang, H. H. Lee, H. T. Chen, and T. L. Liu, "Text-guided graph neural networks for referring 3D instance segmentation," in *AAAI*, vol. 35, no. 2, 2021, pp. 1610–1618. [8](#), [15](#)
- [123] M. Feng, Z. Li, Q. Li, L. Zhang, X. Zhang, G. Zhu, H. Zhang, Y. Wang, and A. Mian, "Free-form description guided 3D visual graph network for object grounding in point cloud," in *CVPR*, 2021, pp. 3722–3731. [9](#), [15](#)
- [124] Z. Yuan, X. Yan, Y. Liao, R. Zhang, S. Wang, Z. Li, and S. Cui, "InstanceRefer: Cooperative holistic understanding for visual grounding on point clouds through instance multi-level contextual referring," in *CVPR*, 2021, pp. 1791–1800. [9](#), [15](#)
- [125] J. Roh, K. Desingh, A. Farhadi, and D. Fox, "LanguageRefer: Spatial-language model for 3D visual grounding," in *CoRL*, 2022, pp. 1046–1056. [9](#)
- [126] J. Devlin, M. W. Chang, K. Lee, and K. Toutanova, "BERT: Pre-training of deep bidirectional transformers for language understanding," *arXiv preprint arXiv:1810.04805*, 2018. [9](#)
- [127] L. Zhao, D. Cai, L. Sheng, and D. Xu, "3DVG-Transformer: Relation modeling for visual grounding on point clouds," in *ICCV*, 2021, pp. 2928–2937. [9](#), [15](#)
- [128] D. He, Y. Zhao, J. Luo, T. Hui, S. Huang, A. Zhang, and S. Liu, "TransRefer3D: Entity-and-relation aware transformer for fine-grained 3D visual grounding," in *ACM MM*, 2021, pp. 2344–2352. [9](#)
- [129] S. Huang, Y. Chen, J. Jia, and L. Wang, "Multi-view transformer for 3D visual grounding," in *CVPR*, 2022, pp. 15 524–15 533. [9](#), [15](#)
- [130] Z. Yang, S. Zhang, L. Wang, and J. Luo, "SAT: 2D semantics assisted training for 3D visual grounding," in *ICCV*, 2021, pp. 1856–1866. [9](#), [15](#)
- [131] E. Bakr, Y. Alsaedy, and M. Elhoseiny, "Look around and refer: 2d synthetic semantics knowledge distillation for 3d visual grounding," *NeurIPS*, vol. 35, pp. 37 146–37 158, 2022. [9](#)
- [132] S. Chen, H. Zhu, X. Chen, Y. Lei, G. Yu, and T. Chen, "End-to-end 3D dense captioning with Vote2Cap-DETR," in *CVPR*, 2023, pp. 11 124–11 133. [10](#)
- [133] A. Jain, N. Gkanatsios, I. Mediratta, and K. Fragkiadaki, "Bottom up top down detection transformers for language grounding in images and point clouds," in *ECCV*, 2022, pp. 417–433. [9](#), [15](#)
- [134] A. Kamath, M. Singh, Y. LeCun, G. Synnaeve, I. Misra, and N. Carion, "MDETR-modulated detection for end-to-end multi-modal understanding," in *CVPR*, 2021, pp. 1780–1790. [9](#)
- [135] L. H. Li, P. Zhang, H. Zhang, J. Yang, C. Li, Y. Zhong, L. Wang, L. Yuan, L. Zhang, J. N. Hwang *et al.*, "Grounded language-image pre-training," in *CVPR*, 2022, pp. 10 965–10 975. [9](#)
- [136] Y. Wu, X. Cheng, R. Zhang, Z. Cheng, and J. Zhang, "EDA: Explicit text-decoupling and dense alignment for 3D visual grounding," in *CVPR*, 2023, pp. 19 231–19 242. [10](#), [15](#)
- [137] O. Vinyals, A. Toshev, S. Bengio, and D. Erhan, "Show and tell: A neural image caption generator," in *CVPR*, 2015, pp. 3156–3164. [10](#)
- [138] X. Chen and C. Lawrence Zitnick, "Mind's eye: A recurrent visual representation for image caption generation," in *CVPR*, 2015, pp. 2422–2431. [10](#)

- [139] Q. Wu, C. Shen, L. Liu, A. Dick, and A. Van Den Hengel, "What value do explicit high level concepts have in vision to language problems?" in *CVPR*, 2016, pp. 203–212. [10](#)
- [140] Y. Jiao, S. Chen, Z. Jie, J. Chen, L. Ma, and Y.-G. Jiang, "MORE: Multi-order relation mining for dense captioning in 3D scenes," in *ECCV*, 2022, pp. 528–545. [10](#), [15](#)
- [141] H. Wang, C. Zhang, J. Yu, and W. Cai, "Spatiality-guided transformer for 3D dense captioning on point clouds," *arXiv preprint arXiv:2204.10688*, 2022. [10](#), [15](#)
- [142] Z. Yuan, X. Yan, Y. Liao, Y. Guo, G. Li, S. Cui, and Z. Li, "X-Trans2Cap: Cross-modal knowledge transfer using transformer for 3D dense captioning," in *CVPR*, 2022, pp. 8563–8573. [10](#)
- [143] I. Misra, R. Girdhar, and A. Joulin, "An end-to-end transformer model for 3D object detection," in *CVPR*, 2021, pp. 2906–2917. [10](#), [15](#)
- [144] X. Ma, S. Yong, Z. Zheng, Q. Li, Y. Liang, S.-C. Zhu, and S. Huang, "SQA3D: Situated question answering in 3D scenes," *arXiv preprint arXiv:2210.07474*, 2022. [11](#), [13](#), [16](#)
- [145] T. Brown, B. Mann, N. Ryder, M. Subbiah, J. D. Kaplan, P. Dhariwal, A. Neelakantan, P. Shyam, G. Sastry, A. Askell *et al.*, "Language models are few-shot learners," *NeurIPS*, vol. 33, pp. 1877–1901, 2020. [11](#), [16](#)
- [146] D. Khashabi, S. Min, T. Khot, A. Sabharwal, O. Tafjord, P. Clark, and H. Hajishirzi, "UnifiedQA: Crossing format boundaries with a single QA system," *arXiv preprint arXiv:2005.00700*, 2020. [11](#), [16](#)
- [147] A. X. Chang, T. Funkhouser, L. Guibas, P. Hanrahan, Q. Huang, Z. Li, S. Savarese, M. Savva, S. Song, H. Su *et al.*, "ShapeNet: An information-rich 3D model repository," *arXiv preprint arXiv:1512.03012*, 2015. [11](#)
- [148] K. Chen, C. B. Choy, M. Savva, A. X. Chang, T. Funkhouser, and S. Savarese, "Text2Shape: Generating shapes from natural language by learning joint embeddings," in *ACCV*, 2019, pp. 100–116. [11](#)
- [149] A. Radford, J. W. Kim, C. Hallacy, A. Ramesh, G. Goh, S. Agarwal, G. Sastry, A. Askell, P. Mishkin, J. Clark *et al.*, "Learning transferable visual models from natural language supervision," in *ICML*, 2021, pp. 8748–8763. [11](#), [12](#)
- [150] R. Rombach, A. Blattmann, D. Lorenz, P. Esser, and B. Ommer, "High-resolution image synthesis with latent diffusion models," in *CVPR*, 2022, pp. 10 684–10 695. [11](#)
- [151] C. Schuhmann, R. Beaumont, R. Vencu, C. Gordon, R. Wightman, M. Cherti, T. Coombes, A. Katta, C. Mullis, M. Wortsman *et al.*, "LAION-5B: An open large-scale dataset for training next generation image-text models," in *NeurIPS*, vol. 35, 2022, pp. 25 278–25 294. [11](#)
- [152] R. Fridman, A. Abecasis, Y. Kasten, and T. Dekel, "SceneScape: Text-driven consistent scene generation," *arXiv preprint arXiv:2302.01133*, 2023. [11](#)
- [153] L. Höllein, A. Cao, A. Owens, J. Johnson, and M. Nießner, "Text2Room: Extracting textured 3D meshes from 2D text-to-image models," *arXiv preprint arXiv:2303.11989*, 2023. [11](#)
- [154] H. Kato, Y. Ushiku, and T. Harada, "Neural 3d mesh renderer," in *CVPR*, 2018, pp. 3907–3916. [11](#)
- [155] B. Mildenhall, P. P. Srinivasan, M. Tancik, J. T. Barron, R. Ramamoorthi, and R. Ng, "NeRF: Representing scenes as neural radiance fields for view synthesis," *CACM*, vol. 65, no. 1, pp. 99–106, 2021. [11](#)
- [156] B. Poole, A. Jain, J. T. Barron, and B. Mildenhall, "DreamFusion: Text-to-3D using 2D diffusion," *arXiv preprint arXiv:2209.14988*, 2022. [11](#)
- [157] M. A. Bautista, P. Guo, S. Abnar, W. Talbott, A. Toshev, Z. Chen, L. Dinh, S. Zhai, H. Goh, D. Ulbricht *et al.*, "GAUDI: A neural architect for immersive 3D scene generation," *NeurIPS*, vol. 35, pp. 25 102–25 116, 2022. [11](#)
- [158] J. Ho, A. Jain, and P. Abbeel, "Denoising diffusion probabilistic models," in *NeurIPS*, vol. 33, 2020, pp. 6840–6851. [11](#)
- [159] R. Po and G. Wetzstein, "Compositional 3D scene generation using locally conditioned diffusion," *arXiv preprint arXiv:2303.12218*, 2023. [11](#)
- [160] D. Cohen-Bar, E. Richardson, G. Metzger, R. Giryes, and D. Cohen-Or, "Set-the-Scene: Global-local training for generating controllable nerf scenes," *arXiv preprint arXiv:2303.13450*, 2023. [11](#)
- [161] S. Peng, K. Genova, C. Jiang, A. Tagliasacchi, M. Pollefeys, T. Funkhouser *et al.*, "OpenScene: 3D scene understanding with open vocabularies," in *CVPR*, 2023, pp. 815–824. [12](#)
- [162] J. Zhang, R. Dong, and K. Ma, "CLIP-FO3D: Learning free open-world 3D scene representations from 2D dense CLIP," *arXiv preprint arXiv:2303.04748*, 2023. [12](#)
- [163] R. Chen, Y. Liu, L. Kong, X. Zhu, Y. Ma, Y. Li, Y. Hou, Y. Qiao, and W. Wang, "CLIP2Scene: Towards label-efficient 3D scene understanding by CLIP," in *CVPR*, 2023, pp. 7020–7030. [12](#)
- [164] X. Dong, J. Bao, Y. Zheng, T. Zhang, D. Chen, H. Yang, M. Zeng, W. Zhang, L. Yuan, D. Chen *et al.*, "MaskCLIP: Masked self-distillation advances contrastive language-image pretraining," in *CVPR*, 2023, pp. 10 995–11 005. [12](#)
- [165] J. Yang, R. Ding, Z. Wang, and X. Qi, "RegionPLC: Regional point-language contrastive learning for open-world 3D scene understanding," *arXiv preprint arXiv:2304.00962*, 2023. [12](#)
- [166] D. Cai, L. Zhao, J. Zhang, L. Sheng, and D. Xu, "3DJCG: A unified framework for joint dense captioning and visual grounding on 3D point clouds," in *CVPR*, 2022, pp. 16 464–16 473. [12](#), [15](#)
- [167] Z. Jin, M. Hayat, Y. Yang, Y. Guo, and Y. Lei, "Context-aware alignment and mutual masking for 3D-language pre-training," in *CVPR*, 2023, pp. 10 984–10 994. [12](#), [15](#), [16](#)
- [168] H. Caesar, V. Bankiti, A. H. Lang, S. Vora, V. E. Liong, Q. Xu, A. Krishnan, Y. Pan, G. Baldan, and O. Beijbom, "nuScenes: A multimodal dataset for autonomous driving," in *CVPR*, 2020, pp. 11 621–11 631. [13](#)
- [169] X. Chen, T. Zhang, Y. Wang, Y. Wang, and H. Zhao, "FUTR3D: A unified sensor fusion framework for 3D detection," in *CVPR*, 2023, pp. 172–181. [14](#)
- [170] R. Padilla, S. L. Netto, and E. A. Da Silva, "A survey on performance metrics for object-detection algorithms," in *ICSSIP*, 2020, pp. 237–242. [13](#)
- [171] R. Vedantam, C. Lawrence Zitnick, and D. Parikh, "CIDEr: Consensus-based image description evaluation," in *CVPR*, 2015, pp. 4566–4575. [13](#)
- [172] K. Papineni, S. Roukos, T. Ward, and W.-J. Zhu, "BLEU: a method for automatic evaluation of machine translation," in *ACL*, 2002, pp. 311–318. [13](#), [14](#)
- [173] S. Banerjee and A. Lavie, "METEOR: An automatic metric for MT evaluation with improved correlation with human judgments," in *ACLW*, 2005, pp. 65–72. [13](#)
- [174] C. Y. Lin, "ROUGE: A package for automatic evaluation of summaries," in *Text summarization branches out*, 2004, pp. 74–81. [13](#)
- [175] P. Rajpurkar, J. Zhang, K. Lopyrev, and P. Liang, "SQuAD: 100,000+ questions for machine comprehension of text," *arXiv preprint arXiv:1606.05250*, 2016. [14](#)
- [176] P. Anderson, B. Fernando, M. Johnson, and S. Gould, "SPICE: Semantic propositional image caption evaluation," in *ECCV*, 2016, pp. 382–398. [14](#)
- [177] B. Lester, R. Al-Rfou, and N. Constant, "The power of scale for parameter-efficient prompt tuning," *arXiv preprint arXiv:2104.08691*, 2021. [16](#)
- [178] E. J. Hu, Y. Shen, P. Wallis, Z. Allen-Zhu, Y. Li, S. Wang, L. Wang, and W. Chen, "LoRA: Low-rank adaptation of large language models," *arXiv preprint arXiv:2106.09685*, 2021. [16](#)
- [179] B. Zhuang, C. Shen, M. Tan, L. Liu, and I. Reid, "Towards effective low-bitwidth convolutional neural networks," in *CVPR*, 2018, pp. 7920–7928. [17](#)
- [180] Z. Zhuang, M. Tan, B. Zhuang, J. Liu, Y. Guo, Q. Wu, J. Huang, and J. Zhu, "Discrimination-aware channel pruning for deep neural networks," in *NeurIPS*, vol. 31, 2018. [17](#)
- [181] N. Kitaev, E. Kaiser, and A. Levskaya, "Reformer: The efficient transformer," *arXiv preprint arXiv:2001.04451*, 2020. [17](#)
- [182] T. Dao, D. Y. Fu, S. Ermon, A. Rudra, and C. Ré, "FlashAttention: Fast and memory-efficient exact attention with IO-awareness," in *NeurIPS*, 2022. [17](#)
- [183] J. Li, D. Li, S. Savarese, and S. Hoi, "BLIP-2: Bootstrapping language-image pre-training with frozen image encoders and large language models," *arXiv preprint arXiv:2301.12597*, 2023. [17](#)